ANNUAL REVIEWS

Annual Review of Fluid Mechanics

Linear Flow Analysis Inspired by Mathematical Methods from Quantum Mechanics

Luca Magri,[1] Peter J. Schmid,[2] and Jonas P. Moeck[3]

[1]Department of Aeronautics, Imperial College London, London, United Kingdom; email: l.magri@imperial.ac.uk

[2]Department of Mechanical Engineering, King Abdullah University of Science and Technology (KAUST), Thuwal, Saudi Arabia

[3]Department of Energy and Process Engineering, Norwegian University of Science and Technology, Trondheim, Norway

Annu. Rev. Fluid Mech. 2023. 55:541–74

First published as a Review in Advance on October 20, 2022

The *Annual Review of Fluid Mechanics* is online at fluid.annualreviews.org

https://doi.org/10.1146/annurev-fluid-031022-044209

Keywords

linear analysis, quantum mechanics, symmetries, degeneracy, perturbations, exceptional points, spectral analysis, eigenvalues, stability

Abstract

Since its birth in the 1920s, quantum mechanics has motivated and advanced the analysis of linear operators. In this effort, it significantly contributed to the development of sophisticated mathematical tools in spectral theory. Many of these tools have also found their way into classical fluid mechanics and enabled elegant and effective solution strategies as well as physical insights into complex fluid behaviors. This review provides supportive evidence for synergistically adopting mathematical techniques beyond the classical repertoire, both for fluid research and for the training of future fluid dynamicists. Deeper understanding, compelling solution methods, and alternative interpretations of practical problems can be gained by an awareness of mathematical techniques and approaches from quantum mechanics. Techniques such as spectral analysis, series expansions, considerations on symmetries, and integral transforms are discussed, and applications from acoustics and incompressible flows are presented with a quantum mechanical perspective.

1. HISTORY AND MOTIVATION

Planck's relation: the energy of a photon is $\hbar\omega$, where ω is the angular frequency and $\hbar \approx 1.054571817 \times 10^{-34}$ J·s is Planck's constant (divided by 2π)

Although the majority of physical phenomena involve nonlinear processes and mechanisms, most scientific inquiries into nonlinear behavior deploy linear tools to quantify, analyze, and examine their overall role and mutual interactions. Linear stability has remained a powerful mathematical tool to gain understanding of fluid behavior by tracking infinitesimal perturbations or observing responses to forcing. Comprehensive reviews have periodically summarized the development of new tools and the rise of new research directions over the past decades, including Stuart (1971), who gave an early account of mathematical methods for stability theory with an extension to incorporate nonlinear effects; Huerre & Monkewitz (1990), who reviewed the distinction between convective and absolute instabilities; Chomaz (2005) and Theofilis (2011), who expanded linear stability beyond the parallel-flow assumption; and Schmid (2007), who discussed nonmodal stability analysis to capture a finite-time, rather than asymptotic, evolution of linear perturbations—a mathematical framework that has recently been extended to account for nonlinearities, as reviewed by Kerswell (2018). A frequency-based approach using input–output or resolvent analysis has been reviewed by Jovanović (2021). Luchini & Bottaro (2014) surveyed the applicability and use of adjoint techniques to perform quantitative flow analysis based on a sensitivity and optimization approach. Applications of these linear, and recent nonlinear, tools include, among others, the stability and transition characteristics of high-speed boundary layers using modal receptivity and spectral analyses (Fedorov 2011), as well as the behavior of thermoacoustic systems (Juniper & Sujith 2018), their extreme sensitivity to small perturbations, and their optimal design using adjoint methods (Magri 2019). Many techniques routinely used in the analysis of fluid systems have their origin in quantum mechanics. Above all, the custom of describing the behavior of a flow by the spectral properties of the underlying evolution operator has its roots in quantum physics, where eigenvalues of operators have been used to represent discrete energy levels and to quantize physical systems. For example, quantization is employed in pilot-wave theories of bouncing droplets (Couder et al. 2005, Bush 2015). While there is much overlap in techniques between fluid dynamics and quantum mechanics, some methods had to undergo modifications to adapt to the particularities of fluid systems, such as nonnormal evolution operators (Trefethen et al. 1993) or nonlinear eigenvalue problems, as encountered in acoustics (Magri 2019).

This review is based on mathematical techniques arising from quantum mechanics (e.g., Dirac et al. 1930, Birkhoff & Von Neumann 1936, Griffiths 1995). As such, it is fitting to first give a brief historical sketch of key developments and milestones. In 1900, Max Planck modeled the black body radiation under the assumption that the radiated energy does not vary continuously, but instead takes on discrete values. Planck observed that light radiation behaves as if the energy exchanged with a black body occurs in quanta—indivisible parcels of energy. Planck's relation reconciled theoretical predictions with experimental observations, but only partly offered a physical interpretation. In 1905, Albert Einstein took Planck's hypothesis to a physical level. He postulated that light radiation consists of a beam of corpuscles (photons) with discrete energy, and his research on the associated photoelectric effect won him the Nobel Prize in Physics in 1921. On the one hand, Einstein's quantum hypothesis firmly established the photon (corpuscular) theory of light and later helped explain the scattering of a photon by a charged particle (the Compton effect). On the other hand, the hypothesis of light particles encountered difficulties in all cases of interference and diffraction (e.g., Young's double slit experiment), where a wave theory was more successful. This dichotomy made the duality of light (corpuscular/wave-like) one of the most fascinating puzzles in modern physics, which was ultimately resolved by positing that light propagates as a wave but manifests its corpuscular nature only at the instant of detection. To explain the existence of the wave–corpuscle duality, which was subsequently also observed in matter such as

BRA–KET NOTATION

Bra–ket notation is a convention introduced by Paul Dirac in 1939 to denote quantum states: A ket, $|\cdot\rangle$, is a vector, and a bra, $\langle\cdot|$, is the vector dual to the ket. In a finite-dimensional space, a ket can be represented as a column vector, and a bra can be represented by a row vector.

electrons, atomic systems, and molecules (i.e., matter waves), in 1913 Niels Bohr postulated the quantization of atoms: An atom can only exist in a certain number of stationary states (or quantum states), each with a well-defined energy, and transitions between those states can only be accomplished by jumps of discrete energy values. This hypothesis successfully explained line spectra and was later experimentally verified by Franck and Hertz.

From a mathematical point of view, the foundations of quantum mechanics renewed interest in linear operators and spectral theory (Steen 1973), a mathematical field also underlying the linear analysis of fluid flows. A fundamental theorem from spectral theory that plays a major role in quantum mechanics is the Riesz representation theorem, which provides the mathematical foundation of the popular bra–ket notation. Broadly put, the theorem states that every bra, $\langle\cdot|$, has a corresponding and unique ket, $|\cdot\rangle$ (see the sidebar titled Bra–Ket Notation). In fluid mechanics, the Riesz theorem forms the basis of the widespread direct-adjoint framework (e.g., Luchini & Bottaro 2014, Magri 2019). A second fundamental theorem from spectral theory that plays a major role is the spectral theorem. Under mild assumptions, as shown by David Hilbert and Frigyes Riesz, bounded linear operators can be represented in diagonal form as a summation over the point spectrum and as an integral over the continuous spectrum.

While quantum mechanics benefited from a body of literature on spectral theory, it also had a substantial influence on spectral theory with the two different formalisms, that of Heisenberg, Born, and Jordan and that of Schrödinger. Both approaches rely on linear operators and their spectra: The matrix approach (Heisenberg, Born, and Jordan; 1925–1926) represents each physical quantity by a linear operator, leading to a formalism known as matrix mechanics, and the wave-mechanics approach of Schrödinger uses partial differential equations and yields the so-called wave-mechanics formulation. These two approaches were shown to be two representations of a more general unified theory by Dirac. Another important advance came with a spectral theory based on an abstract definition of a linear operator on a Hilbert space by von Neumann (1927); it paved the way for the analysis of self-adjoint operators as they arise in quantum mechanics. A later generalization to normal operators (i.e., operators that commute with their adjoints) generalized von Neumann's original work. These new theories challenged the role of classical mechanics, which had successfully explained phenomena at large scales over centuries (using, e.g., Newtonian mechanics for nonrelativistic speeds). Bohr postulated that classical theory is macroscopically correct—it accurately predicts phenomena in the limit where quantum discontinuities can be considered infinitesimally small. Notably, classical wave theory was still able to predict the average value of quantum observables, such as momentum and position (as expressed in the correspondence principle by Paul Ehrenfest).

Recently, tools from quantum mechanics have been successfully adopted, and extended, by fluid mechanicians. These tools have been employed both to assess fundamental fluid phenomena and to tackle engineering challenges in aero- and thermoacoustics of turbines and combustors, in flow instabilities, and in active swimmers, to name a few. By way of examples and applications in acoustics and incompressible flows, the objectives of this review are to (*a*) bridge the gap between common tools used in the quantum mechanics and fluid mechanics communities; (*b*) show mathematical connections, analogies, and differences; (*c*) provide alternative solution strategies

Matter waves: De Broglie relations link the momentum, p, of a particle with mass with the wavelength, λ, according to $p = 2\pi\hbar/\lambda$

Exceptional point: degeneracy in non-Hermitian systems where eigenvalues and associated eigenfunctions coalesce (branch-point singularities in the parameter space), in which the eigenvalue sensitivity is infinite; thus, the parameter dependence is given by a Puiseux series

and analysis frameworks; (*d*) review scientific examples and practical applications; and (*e*) identify a variety of other areas in fluid dynamics that may benefit from and, in turn, generalize mathematical techniques from quantum mechanics. All fluids examples addressed in this review belong to the realm of classical physics. The connection to quantum mechanics is mathematical and procedural in nature. The review is structured as follows. We first address formulation and fundamentals (Section 2), where the basic connections, analogies, and differences between quantum mechanics and linearized fluids are explained. We then treat symmetries and symmetry-breaking (Section 3) and review recent developments and progress in symmetry-breaking in fluids, PT (parity–time) symmetries, and exceptional points. This is followed by series expansions (Section 4), where different types of expansions and various approximations of spectral properties are surveyed. Section 5 gives a brief exposition of deriving rheological models from quantum mechanical analogs of many-body systems. All of these topics are connected by linearity as the common factor. Application areas include incompressible flows, aeroacoustics, thermoacoustics, active fluids, and numerical methods.

2. FORMULATION AND FUNDAMENTALS

In the classical world of fluids, an experiment can determine the state of a flow system. In the quantum world, this is no longer true. The principles underlying linear flows, and generally classical mechanics, are profoundly different from those of quantum systems (see **Table 1**). In classical linear flows, (*a*) the state of a system is completely defined by its coordinates and its momentum, and while the linear flow state can be represented by a complex number when Laplace transformed, it is physically a real quantity; (*b*) a measurement of a physical quantity is entirely determined by the state of the system (i.e., the result of any measurement can be predicted with certainty, to experimental accuracy, if the state of the system is fully known); and (*c*) the time evolution of the flow state is governed by deterministic equations. These are typically based on nonnormal operators, such as the linearized Navier–Stokes equations. In contrast, in quantum mechanics, (*a*) the state of the system is defined by a wave function, which is a complex normalizable quantity; (*b*) the possible results of a measurement, which must be real numbers, are given by the eigenvalues of the linear operator that represents the observables; (*c*) the temporal evolution of the state vectors is unitary (hence normal), governed by the Schrödinger equation; and (*d*) the eigenstates are orthogonal. The inner product between two states thus serves as a measure of the inability to distinguish them with certainty, and the outcome probability of an experiment is given by the square of the inner product between an eigenstate and the state (in nondegenerate cases). The consequences of

Table 1 Principles, analogies and differences between quantum mechanics and linear flow analysis

	Quantum mechanics	Linear flow analysis
Observable	Linear operator	Flow state
Measurement	Eigenvalue of observable	Value of state
Outcome of measurements	Intrinsically probabilistic	Deterministic
Time evolution	Unitary operator	Nonunitary
Eigenfunctions	Orthogonal	Nonorthogonal
Eigenvalues/spectrum	Real	Complex
Governing equation	Heuristic, normal	Linearization of conservation laws, nonnormal
Solution (dual solution)	Ket (bra), $\lvert\psi\rangle$ ($\langle\psi\rvert$)	Direct (adjoint), ψ (ψ^+)

these fundamental principles are twofold. First, quantum operators that represent observables are traditionally Hermitian on Hilbert spaces (see Section 3.4 for non-Hermitian quantum mechanics), and their spectra represent the values that the associated physical quantity can attain. Second, some physical quantities, such as position and momentum, cannot be determined or measured simultaneously to the same accuracy (Heisenberg's uncertainty principle). Conservation laws (energy, momentum, and mass), however, are still valid in the quantum world (for the nonrelativistic regime, which we assume throughout this review). Another crucial principle of quantum mechanics is the principle of superposition. This principle is based on the fact that the states describing the system appear linearly in the governing equations. Superposition in quantum mechanics, however, is different from the superposition principle in linear flow analysis. On the quantum side, a superposition of two identical states results in the same state, whereas in fluid mechanics a superposition of two identical states produces the same state that is twice as large in magnitude. In other words, the quantum mechanical superposition relates to the probability of observation, while the fluid mechanical superposition addresses the amplitude of the state.

2.1. Two-State Systems

Several fluid problems that are characterized by two distinct states, and cast into two degrees of freedom, can be represented as two-state systems. Systems of this type are commonly rotationally symmetric and found in, for example, acoustically active annular configurations (e.g., Bauerheim et al. 2016), and the flow past certain bluff bodies (e.g., Rigas et al. 2015, 2017). The states in these systems are degenerate (Section 3)—they are orthogonal to each other but oscillate with the same frequency.

The quantum mechanical analog to a two-state system is given by a single qubit (see the sidebar titled Qubit), which represents the superposition of two orthogonal eigenfunctions, $|0\rangle$ (e.g., spin-up) and $|1\rangle$ (e.g., spin-down). We express the qubit as $|\psi\rangle = a|0\rangle + b|1\rangle$, with a and b being complex probability amplitudes of finding the system in either state $|0\rangle$ or state $|1\rangle$, respectively. Any outcome of a measurement identifies one of either state, which introduces a normalization condition for the two quantum states in the form of $|a|^2 + |b|^2 = 1$. As a consequence, the qubit is characterized by two independent real parameters, and geometrically, it lives on a sphere of unit radius:

$$|\psi\rangle = \cos(\chi)|0\rangle + \sin(\chi)\left[\cos(\Delta\phi) + \mathrm{i}\sin(\Delta\phi)\right]|1\rangle, \quad \chi \in [-\pi/2, \pi/2], \ \Delta\phi = [0, 2\pi), \quad 1.$$

where $\Delta\phi$ is the phase difference between the two fundamental states (the absolute phase is arbitrary and cannot be measured). (In quantum mechanics, it is also common to use $\chi \to \chi/2$ and $[-\pi/2, \pi/2] \to [0, \pi]$.) The geometric representation of Equation 1 is referred to as the Bloch sphere (Bloch 1946, Arecchi et al. 1972) (in light polarization, the Bloch sphere is known as the Poincaré sphere). In a spin-1/2 particle, the North pole ($\chi = \pi/2$) represents the spin-up state, whereas the South pole ($\chi = -\pi/2$) describes the spin-down state. The only possible classical states are the poles; for quantum states, any state on the surface of the sphere is admissible.

QUBIT

The qubit is the basic unit of quantum information and the quantum version of the classic (binary) bit. Examples of qubits are spin-up/spin-down, the polarization of a photon, and quantum dots. A classic bit can only take on two values (pure states), while the qubit can assume an infinite number of states given by a linear combination of the pure states.

2.1.1. Annular acoustic instability. As an example of application, the Bloch sphere representation enables physical insight and robust modeling of annular combustors. In typical aero-engine designs, the flame holders are arranged along the mean circumference of an annulus to increase the power density of the machine. These annular configurations are nominally rotationally symmetric (Section 3)—the flames are positioned equidistantly from each other and have, again nominally, the same geometric/fuel characteristics. If the heat released by the flames is sufficiently in phase with the acoustic pressure waves, a thermoacoustic instability can arise (Rayleigh 1878). If uncontrolled or not prevented, azimuthal instabilities saturate into high-amplitude pressure oscillations, which can limit the operating regimes, cause structural damage and fatigue, and, in the worst-case scenario, destroy the engine (or components thereof) (e.g., Candel 2002, Lieuwen & Yang 2005, Culick 2006). In annular combustors, thermoacoustic instabilities can be grouped into (*a*) spinning, if the nodal lines rotate azimuthally like a traveling wave (typical of rotationally symmetric configurations); (*b*) standing, if the nodal lines are statistically stationary with a fixed orientation (more typical of rotationally asymmetric configurations); and (*c*) mixed, if the nodal lines switch between the two former states (typical of weakly asymmetric configurations) (e.g., Schuermans et al. 2006, Noiray et al. 2011, Worth & Dawson 2013). The underlying mechanisms responsible for the dynamic nature of these azimuthal modes are not yet fully understood (Noiray et al. 2011). This has prompted high-fidelity simulations (Wolf et al. 2012), experimental campaigns in atmospheric and pressurized rigs (Bourgouin et al. 2013, Noiray & Schuermans 2013, Worth & Dawson 2013, Ahn et al. 2021, Mazur et al. 2021), and fundamental studies (e.g., Moeck et al. 2010, Noiray et al. 2011, Ghirardo & Juniper 2013, Duran & Morgans 2015, Bauerheim et al. 2016, Laera et al. 2017, Mensah et al. 2019, Murthy et al. 2019).

2.1.2. Representation of instabilities on the Bloch sphere. For the design of effective control strategies to suppress purely azimuthal instabilities, it is essential to establish the nature (spinning, standing, or mixed) of the unstable modes. In this pursuit, experimental data on the acoustic pressure (e.g., from microphones) is postprocessed to classify the modal nature. The pressure in the annulus is a function of the azimuthal coordinate, θ, and time, t, which can be projected onto two orthogonal eigenfunctions, which can be the standing modes

$$p(\theta,t) = \xi_1(t)|\,0\rangle + \xi_2(t)|\,1\rangle \qquad \text{with} \qquad |\,0\rangle \equiv \cos(n\theta), \qquad |\,1\rangle \equiv \sin(n\theta). \qquad 2.$$

Since the acoustic timescale, t, is significantly larger than the timescale over which the envelope of the signal varies, a two-time decomposition is assumed: $\xi_i(t) = A_i(t)\cos[\omega t + \phi_i(t)]$, $i = 1, 2$, where $A_i(t)$ and $\phi_i(t)$ are the slow-varying amplitude and phase, respectively, which are obtained from a Hilbert transform of the temporal pressure signal. As pointed out by Ghirardo & Bothien (2018, section III), the state phase of A_1 and A_2 and and ϕ_1 and ϕ_2 is ill posed, which means that the pressure cannot be reconstructed if we have $A_1 = 0$ or $A_2 = 0$. (Identical conclusions can be drawn if spinning modes are chosen as a basis.) This ambiguity, however, can be resolved by representing the eigenfunctions as a two-state system on a Bloch sphere. In fact, the analytic pressure, p_a, is a complex state that depends on four real parameters (two complex parameters), similar to the qubit. (The real part of the analytic pressure is the pressure, whereas the imaginary part is the Hilbert transform of the pressure.) In contrast to the qubit, the analytic pressure is given by three independent real parameters, as no normalization needs to be imposed. Using a compact formalism, Ghirardo & Bothien (2018) introduced a decomposition for the pressure on the Bloch sphere (**Figure 1*a***),

$$2p(t) = A(t)e^{in[\theta_0(t)-\theta]}e^{-k\chi}e^{i[\omega t+\phi(t)]} + \text{quaternion conjugate} \qquad 3.$$

$$= 2A\left[\cos(\omega t+\phi)\cos(\chi)\cos\left[n(\theta-\theta_0)\right] + \sin(\omega t+\phi)\sin(\chi)\sin\left[n(\theta-\theta_0)\right]\right], \qquad 4.$$

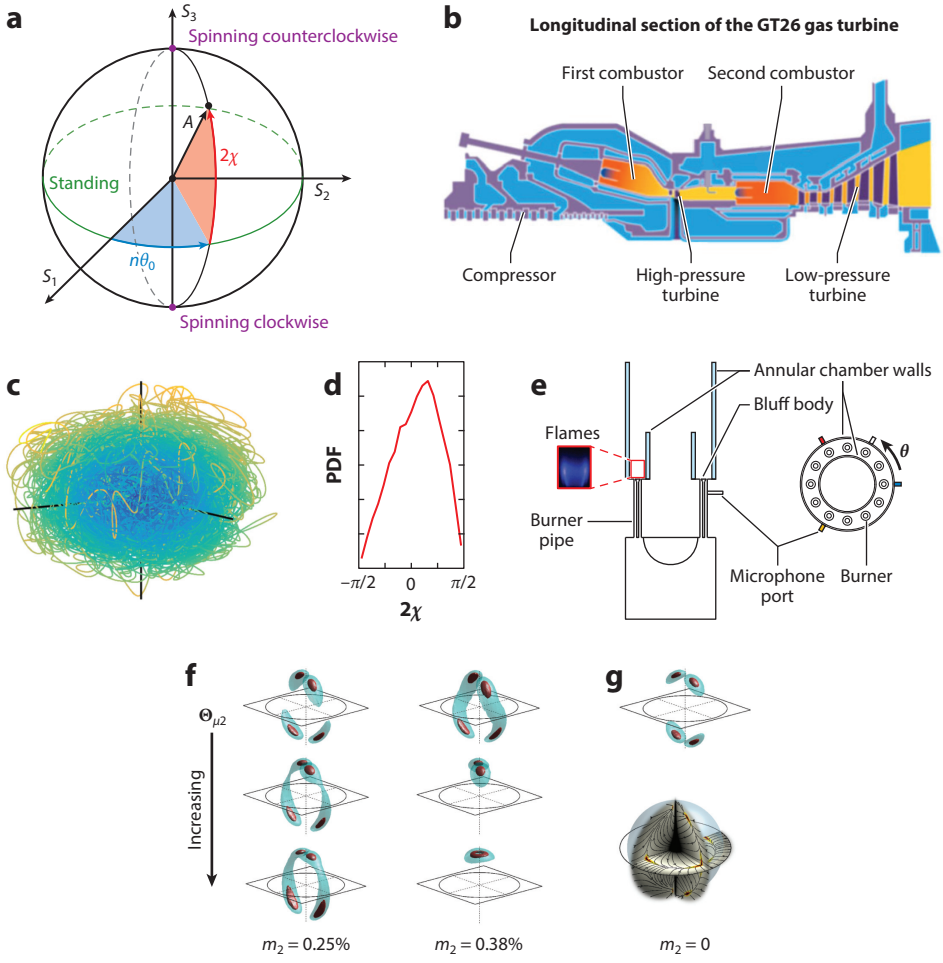

Figure 1

Bloch sphere representation of acoustic azimuthal modes: (*a*) Bloch sphere for azimuthal acoustics. A is the slowly varying amplitude, θ_0 is the orientation angle of the antinodal line, and χ is the nature angle. States at the poles represent pure spinning waves, and states at the equator represent pure standing modes; all other states are mixed. (*b–d*) Nominally rotationally symmetric industrial combustor. (*b*) The industrial annular combustor Ansaldo GT26 gas turbine. (*c*) States on the Bloch sphere. The color of the line qualitatively describes the pressure amplitude A in the second annular combustor in panel *b* for approximately 130,000 acoustic periods. (*d*) Probability density function (PDF) of the nature angle (2χ) for the states in panel *b*, which shows that the industrial combustor is unlikely to be in a spinning state, as the presence of background noise pushes the system away from the poles of the sphere in panel *a*. (*e–g*) Hydrogen-based academic annular combustor. (*e*) The side (*left*) and top (*right*) views of the academic hydrogen–methane annular combustor rig. (*f*) Stationary PDF (25% and 75% probabilities) for purely resistive asymmetry; m_2 is the second-order deviation of the acoustic reactance from the axisymmetric case (chamber geometry, mean flow, temperature, and flame response asymmetries). $\theta_{\mu 2}$ is the orientation of the reactive asymmetry. (*g*) Stationary PDF for resistive and reactive asymmetry. Panels adapted with permission from (*a*) Ghirardo & Bothien (2018), copyright 2018 American Physical Society; (*b*) Ghirardo et al. (2018), copyright 2018 Cambridge University Press; (*c–d*) Ghirardo & Gant (2021), copyright 2021 Elsevier; and (*e–g*) Faure-Beaulieu et al. (2021), copyright 2021 the authors.

where $A = \sqrt{A_1^2 + A_2^2}$ denotes the slowly varying amplitude; $n\theta_0 = [-\pi, \pi)$ is the orientation angle, which is the slowly varying antinodal line of the standing mode; $\chi = [-\pi/2, \pi/2]$ represents the nature angle, which determines the spinning ($\chi = \{-\pi/4, \pi/4\}$) or standing ($\chi = 0$) nature of the mode; and i, j, and k are the quaternion units.

The Bloch sphere representation also offers physical insight into experimental data. Ghirardo & Gant (2019, 2021) studied experimental data from the industrial combustor Ansaldo GT26, which has a first annular combustor connected to a second annular sequential combustor through a high-pressure turbine (**Figure 1*b***). Focusing on the dynamics of the second annular combustor, they concluded that the level of background turbulence, which is modeled as stochastic forcing, affects the dynamics of the fluctuating acoustic fields, making the dynamics slowly drift from the spinning states (represented by the poles of the Bloch sphere) (**Figure 1*c*,*d***). In an academic hydrogen–methane combustor (**Figure 1*e***), Faure-Beaulieu et al. (2021) employed a Bloch sphere representation to physically explain the effect that resistive and reactive asymmetries have on the thermoacoustic dynamics (**Figure 1*f*,*g***), particularly on the azimuthal eigenmodes. Resistive asymmetries arise from nonuniform damping along the annulus, whereas reactive asymmetries prevail in nonaxisymmetric annular combustors and emerge from a nonuniform speed of sound, from a nonuniform reactive component of the flame, or from nonhomogeneous flow responses to acoustic perturbations. The angles $\Theta_{\mu 2}$ and $\Theta_{\alpha 2}$ are the preferential directions of the two types of asymmetries. When $\Theta_{\mu 2} - \Theta_{\alpha 2} \neq 0 \mod \pi/2$, the reflectional symmetry of the system is broken (for example, by a modulation of $\lesssim$1% of the annular cross-sectional area around its circumference). In this case, the resistive and reactive nodal lines are no longer aligned, and we can observe a preference of the system for one spinning direction (corresponding to a preference for a particular hemisphere of the Bloch sphere), even though no mean flow is present.

2.2. Evolution Equations and Path Integrals

Many problems in flow stability can be modeled by equations that have mathematical analogies, but also some differences, with the Schrödinger equation of quantum mechanics. In both quantum mechanics and linear stability, the state evolution is formally governed by

$$\frac{\partial |\boldsymbol{\psi}\rangle}{\partial t} = \mathcal{L}|\boldsymbol{\psi}\rangle, \qquad |\boldsymbol{\psi}\rangle = |\boldsymbol{\psi}_0\rangle \ \text{ at } \ t = 0. \tag{5.}$$

In quantum mechanics, $|\boldsymbol{\psi}\rangle$ represents the state vector (wave function, i.e., ket) and the evolution operator is given as $\mathcal{L} \equiv -i\hbar^{-1}\mathcal{H}$, with $\mathcal{H}$ being the Hamiltonian (see the sidebar titled Notation). The Schrödinger equation can be considered as a postulate of traditional quantum mechanics on the evolution of the quantum state (wave function) (Sakurai & Napolitano 2011). The Schrödinger equation is derived heuristically by imposing wave packet solutions as physically realizable quantities, which enforce De Broglie and Planck relations and the normalization condition that renders the probability of finding a particle somewhere as unity.

NOTATION

To distinguish between quantum mechanics and linear flow analysis, we indicate the quantum state by $|\psi\rangle$ (ket) and the linear flow state by ψ. (Boldface denotes vector functions, e.g., $\boldsymbol{\psi}$.) The linear operator, $\mathcal{L} \equiv -i\hbar^{-1}\mathcal{H}$, is specified according to the context, where the Hamiltonian operator, $\mathcal{H}$, represents the total energy of a system (i.e., the sum of potential and kinetic energies). At nonrelativistic speeds, the Hamiltonian of a particle with mass m is $\mathcal{H} = -\frac{\hbar^2}{2m}\nabla^2 + V$, where V is the potential and ∇^2 is the Laplacian.

On the other hand, in linear flow analysis, the state, ψ, is the linearized state vector (consisting of velocity, pressure, etc.), and $\mathcal{L}$ is the Jacobian of the evolution operator, which represents a first-order approximation of the nonlinear conservation laws (momentum, energy, mass) around a chosen base state. (Boundary conditions are embedded in $\mathcal{L}$ for brevity.) In contrast to quantum mechanics, $\mathcal{L}$ is generally a nonnormal operator (e.g., Schmid 2007). A formal solution of the evolution equation is given by the propagator $\mathcal{U}$, such that

$$|\,\psi(t)\rangle = \mathcal{U}(t_0,t)|\,\psi_0\rangle = \mathcal{P}\left[\exp\left(\int_{t_0}^{t}\mathcal{L}\,\mathrm{d}t\right)\right]|\,\psi_0\rangle, \qquad 6.$$

where the path-ordered integrals, $\mathcal{P}$, are known as the path integrals (Feynman integrals). In quantum mechanics, the propagator is unitary, whereas in linear flow analysis the propagator may not be unitary. The key differences between the linear operators of quantum mechanics and linear flow stability are summarized in **Table 1**.

As an example of application of path integrals, we consider sound generation and indirect noise in gas turbines. In order to reduce the harmful effects of noise pollution generated by aircraft engines, manufacturers are striving to make aeroengines less noisy (Dowling & Mahmoudi 2015, Ihme 2017). While there has been a significant reduction in fan and jet noise, combustion noise, which is generated in the gas turbine combustor, has become a significant acoustic source in aircraft with low-emission engines (Dowling & Mahmoudi 2015). Combustion noise can be generated (*a*) directly by a volumetric expansion caused by the flame, which acts as a monopole source of sound, or (*b*) indirectly by the acceleration of flow inhomogeneities in the nozzle guide vane or turbine blades downstream of the combustor. For decades, indirect noise has posed great challenges for acousticians and gas turbine manufacturers due to the intricate coupling between combustion processes, turbulent mixing, and acoustic radiation (for a review, see Morgans & Duran 2016). Depending on the flow inhomogeneities, indirect noise can further be categorized as entropy noise, when it is generated by temperature inhomogeneities (Marble & Candel 1977), or compositional noise, when it is caused by compositional inhomogeneities (Magri et al. 2016, Magri 2017). Vorticity noise, which is produced by velocity gradients, is typically less significant at low Mach numbers (Howe & Liu 1977, Dowling & Mahmoudi 2015). To predict the correct level of indirect noise, one might employ a divide-and-conquer strategy involving three stages: (*a*) use large-eddy simulations to conduct high-fidelity simulations of the combustion process inside the combustion chamber (**Figure 2*a***), (*b*) extract temperature and compositional inhomogeneities at the combustor's exit and subsequently cross-average them (**Figure 2*b***), and (*c*) solve a low-order acoustic model, which takes as input the flow inhomogeneities and returns the acoustic transfer function (**Figure 2*c*,*d***). As shown by Magri (2017), the equation governing indirect noise for longitudinal acoustic waves is a Schrödinger-like Equation 5 in space, with $t \to x$, with the state $|\boldsymbol{\psi}\rangle \to \hat{\boldsymbol{\mathcal{I}}}$ containing the flow invariants (e.g., mass-flow rate, total enthalpy, entropy, mixture fraction), and with the linear operator $\mathcal{L} \to 2\pi i He\mathbf{A}$, where $\mathbf{A}$ is the inverse of the Jacobian and He is the nondimensional nozzle length (Helmholtz number). After these transformations are identified, the solution is provided exactly by the path integrals (Equation 6), which are termed the Dyson expansion. As shown in **Figure 2**, path integrals were applied to estimate the compositional noise of a realistic aeroengine (Giusti et al. 2017) and, more recently, the noise emitted by realistic nonisentropic nozzles (Jain & Magri 2022). Additionally, the acoustic solution, Equation 6, is equivalent to a Dyson series, which arises in time-dependent perturbation problems in quantum mechanics. In this analogy, the Helmholtz number, He, acts as a perturbation parameter. The path integrals can alternatively be evaluated with a Magnus expansion (Durán et al. 2013, Duran & Morgans 2015), which enables a numerically efficient recursive solution, but the orders are not physically interpretable as perturbation orders. Beyond the realm of acoustics, a variety of

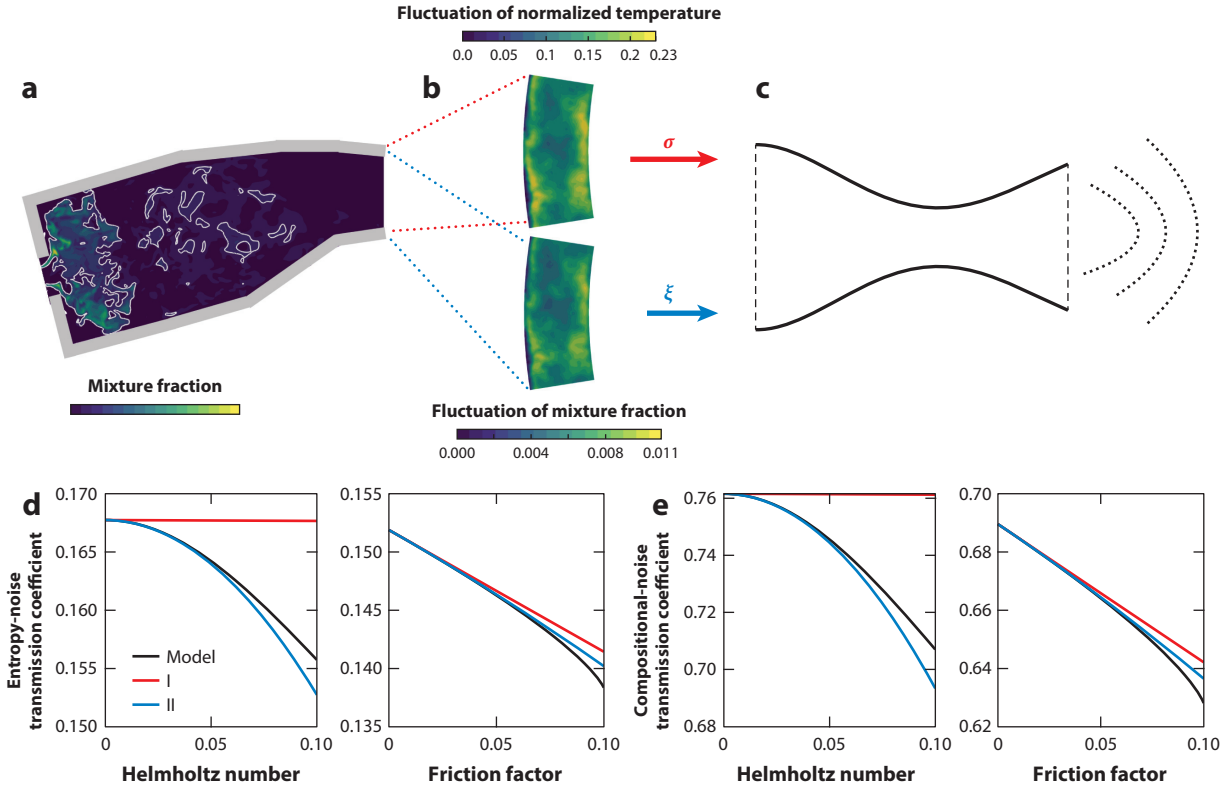

Figure 2

Prediction of indirect noise in a gas turbine using a divide-and-conquer strategy. (*a*) Large-eddy simulation of the turbulent reacting flow in a realistic aeroengine (exact geometry not shown) (Giusti et al. 2017). (*b*) Extraction of flow inhomogeneities from the combustor's exit. Here, σ is the normalized temperature fluctuation and ξ is the mixture fraction fluctuation, which are averaged over the cross section. (*c*) An acoustic model that predicts the acoustic transfer functions for longitudinal waves in the nozzle. The governing equation is a Schrödinger-like equation. (*d*,*e*) Actual calculation from a case with viscous dissipation in the nozzle: acoustic transmission transfer functions of (*d*) temperature inhomogeneities and (*e*) methane compositional inhomogeneities in a nozzle with friction (Jain & Magri 2022). The first (I) and second (II) asymptotic orders are calculated by a path integral.

problems in flow instabilities are governed by Schrödinger-like equations (e.g., Schmid & Henningson 2001).

2.3. Eigenvalue Problems

The evolution Equation 5 can be conveniently analyzed in terms of eigenfunctions and eigenvalues, which are the building blocks of linear operators. This is achieved by separation of variables as $|\psi(t)\rangle = |\hat{\psi}\rangle e^{\lambda t}$ in Equation 5, which, assuming that the linear operator, $\mathcal{L}$, does not depend on time, yields

$$\lambda|\hat{\psi}\rangle = \mathcal{L}|\hat{\psi}\rangle, \qquad 7.$$

where λ represents the eigenvalue and $|\hat{\psi}\rangle$ is the eigenvector. The set of eigenvalues is the spectrum, which in general consists of discrete and continuous subsets. In quantum mechanics, because the linear operator is self-adjoint, the spectrum is real (see Section 3 for a brief reference to non-Hermitian quantum mechanics). For example, the discrete spectrum corresponds to the quantum

energy levels. In linear flow analysis, the mathematical situation is more involved for three reasons. Firstly, linear flow operators are nonnormal; thus, the spectrum is typically complex. The eigenvalues correspond to complex frequencies at which the natural dynamics (eigenfunctions) oscillate about a base state, around which the conservation laws are linearized. Some dynamics may be unstable (positive growth rate), other dynamics may be stable (negative growth rate), or neutrally stable (zero growth rate). Secondly, because of nonnormality, the adjoint problem needs to be solved to analyze the receptivity and sensitivity of the base flow to small perturbations. The adjoint eigenfunction governs the receptivity behavior to linear forcing or initial conditions (Luchini & Bottaro 2014). Thirdly, the complex eigenvalue can appear as part of nonlinear, transcendental terms, yielding a nonlinear eigenvalue problem. This is the case, for example, for some aero-thermoacoustic problems due to the flame's time delay and impedance boundary conditions (Nicoud et al. 2007, Magri 2019), and for some problems related to fluid–structure interaction (Güttel & Tisseur 2017).

Nonlinear eigenvalue problem: defined as $\mathcal{N}(\lambda)\hat{\boldsymbol{\psi}} = 0$, where $\mathcal{N}$ is a linear operator acting on $\hat{\boldsymbol{\psi}}$ that depends nonlinearly on the eigenvalue, λ; linear eigenproblems are common in hydrodynamic stability, in which $\mathcal{N} = \lambda - \mathcal{L}$

3. SYMMETRY AND SYMMETRY-BREAKING

Symmetry and symmetry-breaking are key concepts in theoretical physics and quantum mechanics (see the sidebar titled Symmetry). These concepts have provided elegant and effective solution strategies as well as physical insights. While the role of symmetries for flow dynamics is recognized (e.g., Crawford & Knobloch 1991), their use appears not yet as prevalent as in quantum mechanics. To reduce computational efforts, fluid dynamicists have recently adapted tools from quantum mechanics based on symmetries to tackle engineering problems, such as turbine blade cascades and annular combustion chambers.

With the term "symmetry" one intuitively associates features of an object that remain unchanged when the object is subjected to specific spatial transformations such as rotation or reflection. The notion of symmetry is more general in a mathematical or physical context. Here, a symmetry is understood as a transformation, not necessarily spatial, that leaves an object (a geometrical shape, a function, an equation, or an operator) unchanged. The role of symmetries in physics, and more specifically in fluid dynamics, is manifold. Undoubtedly, the most fundamental aspect is the direct relation between symmetries and conservation laws, as expressed through Noether's theorem (Noether 1918). The most common use in fluid dynamics and related fields is made of scaling symmetries. These are linked to the dimensional homogeneity of physical equations and are routinely exploited to derive similarity laws and similarity solutions (Barenblatt 1996). In a broader mathematical context, similarity solutions are special cases of solution techniques for differential equations based on symmetries (Bluman & Kumei 1996, Cantwell 2002). The present review is concerned with the analysis of linearized fluid systems and their spectral properties and response characteristics; therefore, only the relation between symmetries and these aspects is discussed. Hence, spatial symmetries associated with translations, rotations and reflections are the focus. Only in Section 3.4, we review systems that exhibit PT symmetry, which refers to an invariance with respect to the combined action of parity inversion (flipping one or more coordinates) and time reversal.

SYMMETRY

A symmetry is a transformation that leaves an object unchanged. In the context of spectral theory, a linear operator $\mathcal{L}$ that admits a certain symmetry group commutes with any group element $\mathcal{R}$: $\mathcal{RL} = \mathcal{LR}$; the formal language for analyzing and making use of symmetries is group theory.

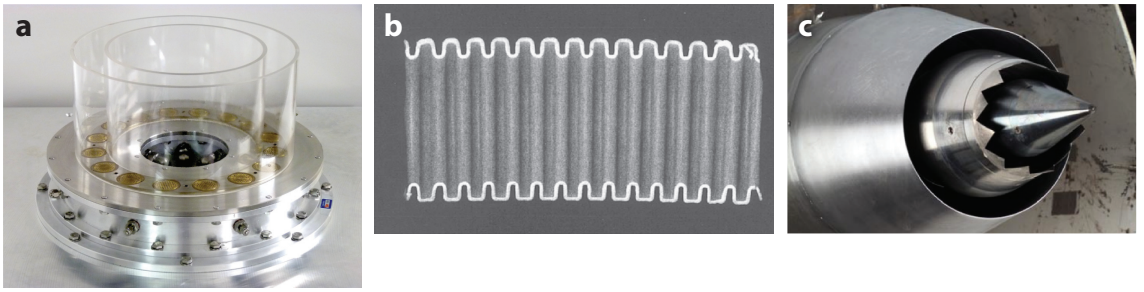

Figure 3

Examples of configurations with discrete spatial symmetries: (*a*) annular combustion chamber, (*b*) corrugated pipe, and (*c*) nozzle with chevrons. Panels adapted with permission from (*a*) Bourgouin et al. (2015), copyright 2014 The Combustion Institute; (*b*) Kristiansen & Wiik (2007), copyright 2007, Acoustical Society of America; and (*c*) Bridges & Wernet (2002), copyright 2002 American Institute of Aeronautics and Astronautics.

We further distinguish between discrete and continuous symmetries. With a continuous symmetry one can associate a parameter, a, that parameterizes the transformation and is arbitrary. For example, axisymmetric systems are invariant with respect to rotations $\theta \mapsto \theta + a$, where θ is an angular coordinate. Here, a is an arbitrary angle because an axisymmetric system is invariant with respect to rotations by any angle. Consider, in contrast, a regular N-gon. This geometrical object is not invariant with respect to rotations by arbitrary angles but only to certain discrete angles, namely, multiples of $2\pi/N$. Therefore, it features a discrete rotational symmetry of order N. The regular N-gon has, moreover, N reflection symmetries. Since reflection symmetries do not involve a continuous parameter, they are discrete symmetries.

There is a multitude of configurations that are relevant to thermofluid systems that feature continuous or discrete symmetries. Scaling symmetries are continuous symmetries because the scaling parameter may be varied continuously. A body of revolution, such as a circular nozzle, features continuous rotational symmetry. The associated flow fields may not exhibit these symmetries after having gone through symmetry-breaking bifurcations (Crawford & Knobloch 1991).

The solution component associated with a continuous spatial symmetry is an exponential, which allows for a normal mode ansatz. An axisymmetric spectral problem, for example, generally admits solutions of the form $\hat{\psi} = \hat{\psi}_m(r, z)e^{im\theta}$, where r, z, and θ are radial, axial, and circumferential coordinates, respectively, and m is an integer. However, the case of discrete spatial symmetries also admits solutions of a particular type—Bloch waves (Floquet modes)—and this can be of great use when studying these systems. **Figure 3** shows systems featuring discrete spatial symmetries. These are invariant with respect to either discrete rotations or discrete translations. Many examples can be found in the fluids domain: compressor or turbine stages, consisting of several identical, equispaced blades; nozzles with chevrons (Rigas et al. 2019), as typically employed in aeroengines, or with other forms of corrugated or lobed structure (Kopiev et al. 2004, Sinha et al. 2016, Schmid et al. 2017, Lajús et al. 2019, Lyu & Dowling 2019); and annular and can-annular combustion chambers frequently encountered in power generation applications and aeroengines, which have been analyzed for their thermoacoustic stability (Mensah et al. 2016, Ghirardo et al. 2019, Murthy et al. 2019, von Saldern et al. 2021). In order for a system to admit a certain spatial symmetry, generally all of the following must be invariant under the transformations associated with the symmetry (group): geometrical configuration, which can be expressed through the boundary conditions; the operator, for example, the linearized Navier–Stokes operator; and the mean field (the explicit coordinate or time dependence), which can be considered part of the operator.

Bloch wave (Floquet mode): eigenfunction or linear response to a spectral problem with discrete spatial symmetry; the product of a Fourier mode and a function that has the same periodicity as the operator

DEGENERATE MODES

The eigenvalue associated with a degenerate mode appears at least twice in the spectrum. In other words, a degenerate mode is found (e.g., via the variation of a parameter) when two eigenvalues coalesce. The nature of a degenerate mode depends on whether, in addition to the eigenvalues, the eigenfunctions also coalesce. Formally, this is expressed through the algebraic and the geometric multiplicity of the eigenvalue. The algebraic multiplicity of an eigenvalue is its order as a zero of the characteristic equation. The geometric multiplicity is the dimension of the associated eigenspace. A degenerate mode, hence, has an algebraic multiplicity that is larger than unity; when the algebraic multiplicity is unity, the eigenvalue is simple. When the geometric multiplicity is equal to the algebraic multiplicity, the eigenvalue is semisimple—it may be degenerate but behaves very much like a simple eigenvalue. When the geometric multiplicity is smaller than the algebraic multiplicity, the eigenvalue is defective. It does not feature the full eigenspace, and this may lead to singularities in the eigenvalue sensitivity and other particular properties (more on these exceptional points in Section 3.4).

Importantly, solutions of a linear stability problem (the eigenfunctions) generally do not need to exhibit the same symmetries as the system. In fact, the eigenfunctions typically exhibit a lower symmetry than the base flow, which inherits the symmetries of the configuration. Consider, for example, the vortex street in the wake of a cylinder. The system features a continuous translation symmetry in time (operator and boundary conditions do not change in time) and a mirror symmetry along a plane parallel to the free stream and passing through the center of the circular cylinder cross section. However, the unstable mode giving rise to the vortex street, which is a solution to this system, does not exhibit either of these symmetries. This is an instance of spontaneous symmetry-breaking where the system undergoes a Hopf bifurcation as a control parameter (here, the Reynolds number) is increased beyond a critical value.

The most prevalent manifestation of spatial symmetry in the eigenstructure of linear operators is twofold: (*a*) the appearance of degenerate modes (see the sidebar titled Degenerate Modes) and (*b*) the emergence of eigenfunctions of a special type. The link between symmetry and eigenvalue degeneracy was extensively explored in the early days of quantum mechanics (Schrödinger 1928), and most elementary textbooks on this subject contain a treatise covering the fundamental aspects (e.g., Griffiths 1995, Sakurai & Napolitano 2011). Since the relation between symmetry and degenerate modes (and everything associated with it) is independent of the underlying physics, it equally applies to quantum and fluid mechanics. Some care has to be exercised, though, because most of the quantum mechanics literature considers self-adjoint systems, as discussed in Section 2. The relation between symmetry and eigenvalue degeneracy is discussed in Section 3.1.

The solution component associated with a continuous spatial symmetry (homogeneity, axisymmetry) is an exponential, the associated wavenumber being restricted through the boundary conditions. When the spatial symmetry is discrete, such as a discrete translation symmetry or a discrete rotational symmetry (see examples in **Figure 3**), the eigenfunctions are not as simple anymore, yet they still feature a special form, namely, that of Bloch waves (also known as Floquet modes). Exploiting the Bloch wave structure of the eigenfunctions for systems with discrete spatial symmetries can be useful for either facilitating a tractable analytical approach or allowing for an efficient numerical solution (Section 3.3).

While traditional quantum mechanics used to be restricted to the analysis of Hermitian systems, specific types of non-Hermitian Hamiltonians, those featuring PT symmetry, have been extensively studied more recently (Bender 2019). This type of Hamiltonian, despite being non-Hermitian, may still feature purely real eigenvalues, a fundamental requirement in quantum

mechanics. When a control parameter is varied beyond a critical value, two eigenvalues collide on the real axis and move into the complex plane, akin to a Hamiltonian Hopf bifurcation (Kirillov 2021). However, in addition to the collision of the eigenvalues, the associated eigenfunctions coalesce as well. This happens at an exceptional point in parameter space, which features intriguing phenomena (Section 3.4).

3.1. Symmetry and Degeneracy

An elementary problem featuring degenerate modes associated with the problem symmetry is the linear stability of laminar flow in a circular pipe (Davey & Salwen 1994). This problem is invariant with respect to transformations belonging to the orthogonal group $O(2)$: rotations around the pipe axis by arbitrary angles and reflection of the angular coordinate. Because of the invariance with respect to rotations in the angular coordinate θ, all eigenfunctions of the relevant linearized set of evolution equations (linearized Navier–Stokes, Orr–Sommerfeld, or similar) are proportional to $e^{im\theta}$, where m is an integer. Because of the invariance with respect to inversion of the angular coordinate, the eigenvalues associated with positive and negative m are identical. All eigenvalues except those corresponding to axisymmetric modes ($m = 0$) are, hence, twofold degenerate. The associated 2D eigenspace is spanned by eigenfunctions proportional to $e^{\pm im\theta}$; however, any element of this eigenspace, such as the two standing modes proportional to $\sin(m\theta)$ and $\cos(m\theta)$, is equally admissible.

There are several important implications associated with eigenvalue degeneracy: (*a*) the indeterminate nature of the mode shape, (*b*) the necessity of a degenerate perturbation expansion (Section 4.1), and (*c*) the splitting of eigenfunctions under asymmetric perturbations. (*a*) Because the eigenspace is (at least) 2D, the nature of the mode shape that would be observed in an experiment is indeterminate. In systems with rotational symmetry, one may therefore generally observe modes rotating in either direction, or standing modes with a nodal line oriented in a certain way (Golubitsky & Stewart 1985, van Gils & Mallet-Paret 1986). However, this cannot be ascertained from a linear analysis; instead, one must resort to weakly nonlinear methods. Thermoacoustic modes in annular combustors (Section 2.1.1) serve as a good example. Since the eigenvalues associated with azimuthal modes are twofold degenerate, and the eigenspace hosts spinning as well as standing modes, the question of which modes would eventually be observed in real systems could not be answered based on linear analysis. Only weakly nonlinear approaches could bring clarity (Noiray et al. 2011, Ghirardo et al. 2016). In these systems, finite-amplitude effects (saturation in the flame response) destabilize standing modes and stabilize spinning modes. The nonlinear system then features two stable limit cycles corresponding to clockwise and counter-clockwise spinning azimuthal modes. (*b*) The parameter dependence of an eigenvalue can be obtained from adjoint perturbation theory. For simple eigenvalues, the leading-order coefficient in a regular perturbation expansion, often referred to as the eigenvalue sensitivity, is well known (Luchini & Bottaro 2014, Magri 2019). However, the routinely used formula is only valid for simple eigenvalues or for degeneracy-preserving perturbations and can lead to erroneous results otherwise (Davey 1978, Davey & Salwen 1994). In general, a degenerate perturbation expansion has to be used, which is detailed in Section 4.1. (*c*) Since symmetry is the cause for degenerate modes to occur, breaking, or reducing, the nominal symmetry of a system may unfold an initially degenerate mode. Reducing the symmetry of the system is typically referred to as explicit symmetry-breaking, which is to be distinguished from spontaneous symmetry-breaking (i.e., the emergence of a state with lower symmetry through an instability of the symmetric base state). Explicit symmetry-breaking may be unintentional and simply result from finite manufacturing precision (**Figure 1**), or it may be intentional, with the goal of affecting the dynamics in a desirable way. In the latter case it is

beneficial to have a fundamental understanding of the effect any introduced asymmetries have and, in particular, of which degenerate modes are split. These aspects are discussed in more detail in Section 3.2.

The wave functions of the hydrogen atom are a fundamental example from quantum mechanics of the appearance of degenerate modes. The energy eigenvalues of the associated Schrödinger equation are degenerate because of the spherical symmetry of this configuration. The symmetries of molecules and crystals are less trivial, and the analysis of the associated degenerate energy levels is commonly conducted based on elements of group theory, which is the formal language for working with symmetries (e.g., Inui et al. 1990).

There is a vast number of fluid configurations commonly analyzed for their spectral properties that feature degenerate modes associated with the problem's symmetries. Davey & Salwen (1994) corrected earlier results from Davey (1978) on the stability of flow in an elliptic pipe. They highlighted the necessity of taking into account the degenerate nature of the eigenvalues when assessing the effect of the pipe's ellipticity on flow stability. In axisymmetric systems, any non-axisymmetric mode is generally degenerate, as it can be rotated by some angle into a linearly independent mode.

As the examples in **Figure 4** show, mode degeneracy is not exclusive to continuous symmetries but may appear in systems with discrete spatial symmetries too. Examples are lobed nozzles or nozzles with chevrons, which are configurations that feature a discrete rotational symmetry of order N, where N is the number of corrugations, and a reflection symmetry in the angular coordinate. As such, degenerate eigenvalues are observed in the spectral analysis of these configurations (e.g., Lajús et al. 2019, Lyu & Dowling 2019). Other prototypical configurations that feature discrete rotational symmetry are those of annular and can-annular combustion chambers found in gas turbines for power generation and propulsion (Noiray et al. 2011, Bauerheim et al. 2016, Magri et al. 2016, Mensah et al. 2019, von Saldern et al. 2021). These systems host N burners equispaced around the central shaft. For these applications, N is typically in the range 10–30. If the azimuthal mean flow, induced by the swirling burner flows, is not too significant, reflection symmetry in the

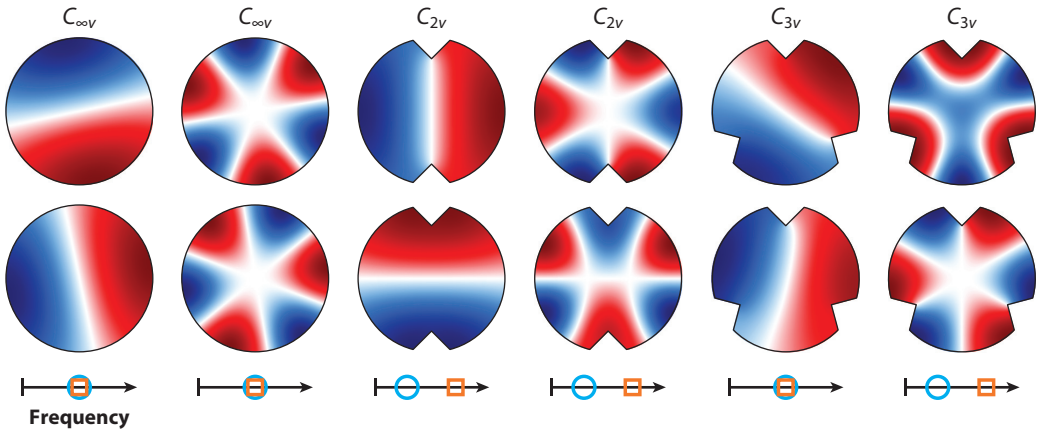

Figure 4

Eigenfunctions of the Helmholtz equation with homogeneous Neumann conditions. Modes of first and third azimuthal order are considered in domains with continuous, twofold, and threefold rotational symmetry, labeled $C_{\infty v}$, C_{2v} and C_{3v}, respectively, according to the Schoenflies notation (e.g., Hamermesh 1989). The symbols on the frequency axis below the eigenfunctions indicate whether the mode is degenerate. If it is degenerate, the two eigenfunctions above span the 2D eigenspace associated with this mode. For a detailed discussion, see sidebar titled Spatial Symmetries and Eigenvalue Degeneracy.

SPATIAL SYMMETRIES AND EIGENVALUE DEGENERACY

Consider an eigenfunction of the Helmholtz equation on a disc (case $C_{\infty v}$ in **Figure 4**), which essentially varies as $\sin(\theta - \theta_0)$. Because this problem features continuous rotational symmetry, indicated by $C_{\infty v}$, the eigenfunction may be rotated by an arbitrary angle (say, $-\pi/2$ to be specific) to yield a new eigenfunction. This new eigenfunction must correspond to the same eigenvalue, as nothing was changed. This new eigenfunction is evidently linearly independent from the initial one. The eigenspace is, hence, at least 2D. It is, in fact, precisely 2D, as any other rotation angle yields a linear combination of the previous two eigenfunctions. In particular, two rotating modes, which vary as $e^{\pm i\theta}$ can be obtained from superposition. The eigenvalue appears twice in the spectrum and, hence, has algebraic multiplicity two, and the dimension of the eigenspace is preserved (i.e., the geometric multiplicity is also two). All of this equally applies to any nonaxisymmetric mode, as for the third-order azimuthal mode shown additionally. However, we cannot make the same argument when the system features only a discrete rotational symmetry of order two, denoted by C_{2v} in **Figure 4**. In fact, reflections along the vertical or horizontal axis or rotations by π only produce linearly dependent versions of the first- and third-order azimuthal modes shown here (or any other mode). Following the same arguments as above, we find that for a configuration with discrete rotational symmetry of order three (C_{3v}), the first-order azimuthal mode remains degenerate but the third-order azimuthal mode appears as a pair of distinct, simple eigenvalues. Considering how an eigenfunction changes under the symmetry transformations often reveals degeneracies. In a group-theoretical framework, degeneracies are identified from the dimension of the irreducible representations associated with the symmetry group (e.g., Inui et al. 1990).

angular coordinate approximately holds. Almost all of the azimuthal combustor modes are then degenerate—more specifically, those whose azimuthal order is not a multiple of $N/2$ (N) if N is even (odd). However, an azimuthal mean flow breaks the reflection symmetry and unfolds the degeneracy (Bauerheim et al. 2015). Eigenvalue degeneracy originating from spatial symmetries is semisimple; that is, the dimension of the eigenspace is preserved, and the sensitivity with respect to parameter variations is finite. Also, in Hermitian systems, defective eigenvalues generally cannot occur; Hermitian degeneracies can, thus, only be semisimple. In non-Hermitian systems without symmetry, however, defective eigenvalues are more common than semisimple eigenvalues because the codimension of the latter is larger than that of the former (Seyranian et al. 2005). Semisimple degenerate modes in systems without spatial symmetries are accidental degeneracies—for example, the vibration modes of triangular membranes for certain angles (Berry & Wilkinson 1984). In Hermitian systems without symmetries, eigenvalue coalescence is unlikely to happen (i.e., without tuning multiple parameters), and this manifests itself in avoided crossings (von Neumann & Wigner 1929).

3.2. Explicit Symmetry-Breaking

Symmetry-breaking can be spontaneous or explicit. Spontaneous symmetry-breaking refers to a reduction in the symmetry of the state (an eigenfunction, for example) while the symmetry of the system (the linear operator) is conserved. In fluid dynamics, spontaneous symmetry-breaking occurs through bifurcations from a base state that has the same symmetry as the system, for example, the onset of periodic vortex shedding from the steady and symmetric flow around a cylinder. The focus of this review is on explicit symmetry-breaking, which can be analyzed with spectral tools originating from quantum mechanics. As discussed in Section 3.1, eigenvalue degeneracy is intimately related to symmetries of the system. Consequently, if the symmetry of the system is reduced through explicit symmetry-breaking, the eigenvalue degeneracies tend to unfold.

Consider an eigenvalue that is two-fold degenerate in the nominal, symmetric system. In quantum mechanics, the hydrogen atom exhibits spherical symmetry and the energy eigenvalues are, therefore, degenerate. Part of this degeneracy is explicitly broken when magnetic or electric fields are applied to break the spherical symmetry. The unfolding of the energy eigenvalues manifests itself as a splitting of the spectral lines (Zeeman and Stark effect). The splitting of degenerate eigenvalues can be predicted with degenerate perturbation theory (Section 4.1), which was introduced by Schrödinger (1928) for the hydrogen atom. In fluid mechanics, the effect of asymmetric perturbations on the frequency and stability of a nominally symmetric system has been the subject of several studies. Davey (1978) and Davey & Salwen (1994) considered the effect of small ellipticity on the stability of pipe flow. They highlighted the importance of taking into account the degenerate nature of the modes when perturbing the eigenstructure of the symmetric (i.e., circular) configuration. To leading order, a small ellipticity was found to be generally destabilizing. A more intricate example of the interplay of symmetry and degeneracy can be found in jets from corrugated nozzles. These systems feature a discrete rotational symmetry of order N, where N is the number of corrugations (lobes or chevrons, for example), including reflection in the angular coordinate, but they do not admit the full $O(2)$ symmetry of the circular jet. Consequently, some, but not all, azimuthal modes split under the effect of the corrugations (Kopiev et al. 2004, Lajús et al. 2019, Lyu & Dowling 2019). Entirely analogous phenomena can be observed in the spectral analysis of thermoacoustic modes in annular and can-annular combustion chambers (Noiray et al. 2011, Ghirardo et al. 2016, Mensah et al. 2019), which nominally feature an N-fold discrete rotational symmetry and can be modeled as two-state systems when only the first azimuthal mode is considered (Section 2). An industrial strategy to passively control acoustic oscillations is based on the introduction of asymmetries along the circumference, which reduces the nominal symmetry of the system and splits some of the degenerate modes. Since the splitting often occurs along the real eigenvalue axis (the oscillation's growth rate), the process is generally destabilizing, as one of the split modes has an increased growth rate. To circumvent this destabilizing effect, the circumferential asymmetry is applied in such a way that the dominant mode's degeneracy is preserved. In stationary gas turbines for power generation, for example, the fuel–air ratio can be varied around the combustor circumference such that the detuning provides a generally stabilizing effect but, at the same time, sufficient symmetry is retained for the targeted mode to remain degenerate (Bothien et al. 2015).

Destabilization by the unfolding of degenerate modes under the effect of asymmetric perturbations commonly occurs in fluids eigenvalue problems due to their non-Hermitian nature. In quantum mechanics, in contrast, where the Hamiltonian is Hermitian, explicit symmetry-breaking leads only to frequency/wavelength splits because the eigenvalues remain real. A quantitative analysis of the effects of explicit symmetry-breaking in spectral fluids problems, therefore, has to be based on adjoint degenerate perturbation theory, as explained in Section 4.1.

3.3. Bloch Waves

The eigenfunctions of problems with discrete spatial symmetries can be represented in the form of Bloch waves, also known as Floquet modes. The alternative terminology that can be found throughout the literature can be attributed to the fact that Floquet's and Bloch's work (Floquet 1883, Bloch 1929) are based on the same mathematical facts. Floquet theory is perhaps more commonly used when the independent variable is time, while Bloch wave theory is more common when it is a spatial coordinate. The work of Bloch can be considered more general, as it covers more complex translation symmetries in three dimensions, such as those found, for example, in crystal structures. Bloch's work specifically addressed problems in quantum mechanics, namely,

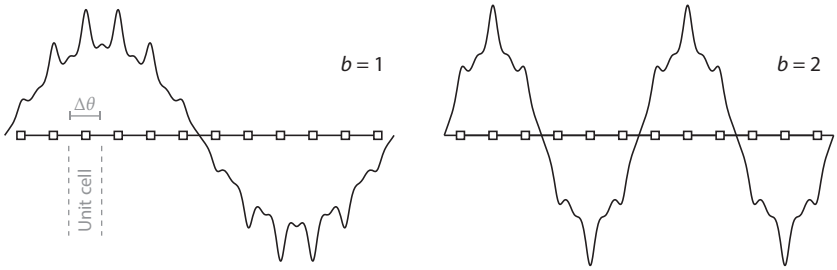

Figure 5

Exemplary illustration of two Bloch waves in a system with discrete rotation/translation symmetry for Bloch wave numbers $b = 1$ and $b = 2$.

finding solutions of the Schrödinger equation for crystal lattices (Kronig & Penney 1931). Hence, we use the term "Bloch wave" in this review.

We concisely illustrate the main aspects of utilizing Bloch wave theory for a system with discrete rotational symmetry. For a translational symmetry in a Cartesian frame, the only difference lies in the set of admissible Bloch wave numbers (denoted b below), which can be determined through the boundary conditions. We consider in the following a system with discrete rotational symmetry of order N, i.e., a system that is assembled from N identical copies of a unit cell of width $\Delta\theta = 2\pi/N$, arranged around the circumference. All eigenfunctions for such a system can be represented as Bloch waves of the form

$$\hat{\psi}_b(r, z, \theta) = u_b(r, z, \theta)e^{ib\theta}. \qquad 8.$$

Here, u_b is periodic in θ with period $2\pi/N$, and b is the Bloch wave number, taking integer values between 0 and $N-1$. A Bloch wave, hence, has the structure of a harmonic modulated by a function that is periodic on the unit cell; see **Figure 5** for an illustration of Bloch waves. In this example with discrete rotational symmetry, the Bloch wave numbers are restricted to a finite set of integers. For systems with discrete translation symmetry, the Bloch wave number can take complex values, which may give rise to band gap phenomena (e.g., Joannopoulos et al. 2008).

If the mode is simple, it is of the form of Equation 8. In case of a semisimple degenerate mode, which, as highlighted earlier, is common in systems with rotational symmetry, the associated eigenspace is (at least) 2D, and not all elements are of the form of Bloch waves. However, there are two Bloch waves that form a basis of the degenerate eigenspace, so that all elements therein can be represented in Bloch form. From the representation of the eigenfunction as a Bloch wave as in Equation 8, two essential properties are evident: (*a*) If the eigenfunction is known on a unit cell, it can be extrapolated to the entire domain via $\hat{\psi}_b(r, z, \theta + n\Delta\theta) = e^{ibn\Delta\theta}\hat{\psi}_b(r, z, \theta)$, with $n = 1 \ldots N-1$. (*b*) The eigenvalue problem can be solved on a unit cell with Bloch-periodic boundary conditions $\hat{\psi}_b(r, z, \theta_0 + \Delta\theta) = e^{ib\Delta\theta}\hat{\psi}_b(r, z, \theta_0)$ for all $b \in \{0, \ldots, N-1\}$. Alternatively, one can use the ansatz in Equation 8 in the original problem to derive an equivalent equation for the periodic part $u_b(r, z, \theta)$. Consider that the original eigenvalue problem is $\mathcal{L}(\lambda; \partial_\theta)\psi = 0$, where λ is the eigenvalue and ψ is the eigenfunction, and the dependence of the operator $\mathcal{L}$ on the other space derivatives is not shown. The equivalent problem for u_b then simply is $\mathcal{L}(\lambda; \partial_\theta + ib)u_b = 0$ on a unit cell, where u_b satisfies periodic boundary conditions in θ. Although we have illustrated here the use of a Bloch wave ansatz for an eigenvalue problem, the same approach is suitable for response analysis too. In this case, the forcing function/boundary condition would be specified in terms of its Bloch wave numbers. When N is large, computations on the unit cell only, rather than for the full configuration, require significantly reduced computational resources.

There exists a variety of problems with discrete spatial symmetries in the fluids domain; consequently, the use of Bloch/Floquet modes finds ample application. In a review on secondary instabilities in boundary layers, Herbert (1988) lays out a Bloch/Floquet ansatz for the eigenvalue problem, where the spatial period in the axial coordinate is the wavelength of the primary instability. In a similar fashion, Moarref & Jovanović (2010) analyzed the effect of streamwise traveling waves on channel flow receptivity, and Ran et al. (2021) studied the effect of riblets on drag reduction with a Bloch/Floquet ansatz [see also the recent review by Jovanović (2021)]. Other recent applications include stability analysis of corrugated jets (Lajús et al. 2019), the calculation of the effective speed of sound in corrugated pipes (Russo et al. 2016), the characterization of acoustic metamaterials (Wu et al. 2018), and thermoacoustic stability analysis of annular and can-annular combustors (Mensah et al. 2016, Ghirardo et al. 2019, Murthy et al. 2019).

3.4. Parity–Time Symmetry and Exceptional Points

A PT-symmetric system is invariant with respect to the simultaneous application of space reflection (parity inversion) and time reversal (Bender 2019). Such systems were suggested by Bender & Boettcher (1998) as an extension to Hermitian quantum mechanics, as they may feature entirely real spectra despite being non-Hermitian. One common feature of PT-symmetric systems and, in fact, of all non-Hermitian systems is the existence of exceptional points in their spectra that can be accessed when one or more parameters are varied (Seyranian et al. 2005, Heiss 2012). At an exceptional point, at least two eigenvalues and their associated eigenfunctions coalesce. To distinguish this from semisimple degeneracies, in which the dimension of the eigenspace is preserved, one also refers to exceptional points as non-Hermitian degeneracies (as they cannot occur in self-adjoint systems). Exceptional points give rise to intriguing behavior and are currently the focus of various fields (Heiss 2012, Doppler et al. 2016, Miri & Alú 2019).

A simple model system featuring PT-symmetry is shown in **Figure 6** and discussed in the sidebar titled Spontaneous Parity–Time Symmetry-Breaking at an Exceptional Point. PT-symmetric systems have been extensively studied during the last decade in various fields, in both quantum and classical systems, highlighting the existence and the theoretically derived properties of exceptional points (Miri & Alú 2019). In the fluids realm, PT-symmetric systems with exceptional points have been realized based on aero- and thermoacoustic experiments (Aurégan & Pagneux 2017, Poignand et al. 2021). Aurégan & Pagneux (2017) utilized a ducted flow configuration with

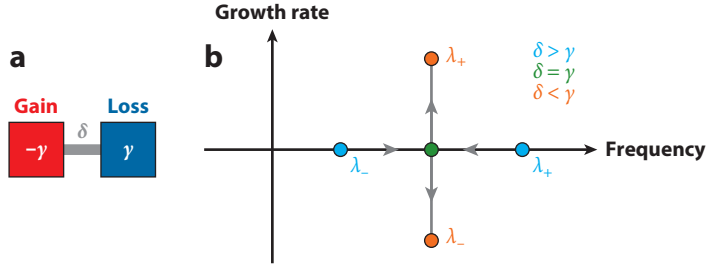

Figure 6

(*a*) Two-state system consisting of a gain and loss subsystem with negative and positive damping γ, respectively. This system is perfectly balanced when the coupling δ is sufficiently large, so that the composite system is neutrally stable and, consequently, has purely real eigenvalues. Conversely, if δ is small compared to γ, the coupling is not sufficiently strong to accommodate a balancing energy transfer; the system is unstable. (*b*) Eigenvalues of the PT-symmetric two-state system as the coupling strength δ is reduced. Abbreviation: PT, parity–time.

SPONTANEOUS PARITY–TIME SYMMETRY-BREAKING AT AN EXCEPTIONAL POINT

Consider a simple model system with two degrees of freedom

$$\mathrm{i}\frac{\partial \boldsymbol{\psi}}{\partial t} = \mathbf{H}\boldsymbol{\psi}, \quad \text{with} \quad \mathbf{H} = \begin{bmatrix} \omega_0 + \mathrm{i}\gamma & \delta \\ \delta & \omega_0 - \mathrm{i}\gamma \end{bmatrix}, \qquad \text{SB1.}$$

which is similar to that discussed by Miri & Alú (2019). This equation represents two subsystems with identical uncoupled resonance frequencies ω_0, coupled through $\delta > 0$ (see **Figure 6*a***). One of the two subsystems has a positive damping rate $\gamma > 0$ (the loss subsystem) and the other has a negative damping rate $-\gamma$ of the same magnitude (the gain subsystem). Time-reversal corresponds to taking the complex conjugate of **H** in Equation SB1; parity inversion merely swaps the two states. The system remains unchanged by applying these two transformations simultaneously. The eigenvalues and eigenvectors of this two-state system are given by $\lambda_\pm = \omega_0 \pm \sqrt{\delta^2 - \gamma^2}$ and $\hat{\boldsymbol{\psi}}_\pm = [-\mathrm{i}\gamma \pm \sqrt{\delta^2 - \gamma^2} \quad \delta]^\mathrm{T}$, respectively. For $\delta > \gamma$ the coupling is sufficiently strong, and gain and loss perfectly balance. The coupled system has then purely real eigenvalues (see **Figure 6*b***); it is said to be in the PT-symmetric phase, and the oscillation amplitudes in the two subsystems are identical. As the coupling, δ, is reduced, the two eigenvalues coalesce at the exceptional point for $\delta = \gamma$, with the two eigenvectors coalescing at this point as well. The eigenvalue at the exceptional point, hence, has algebraic multiplicity two and geometric multiplicity one, and it is therefore defective (**H** is not diagonalizable). Moreover, the exceptional mode is self-orthogonal [i.e., the inner product of direct and adjoint eigenvector vanishes (Heiss 2004, Moiseyev 2011, chapter 9)]. For $\delta < \gamma$ the coupling is not sufficiently strong to achieve a balance between the two subsystems, and the two eigenvalues divert into the complex plane—the system is said to be in the broken phase because the eigenvectors are no longer PT symmetric. The movement of the eigenvalues undergoing a phase transition through the exceptional point is reminiscent of the scenario encountered in a Hamiltonian Hopf bifurcation. Consider now a small perturbation of the coupling constant from the exceptional point toward the broken phase, $\delta = \gamma - \delta'$. The leading-order expansion of the eigenvalues at the exceptional point takes the form of a Puiseux series (Kato 1980, Seyranian & Mailybaev 2003): $\lambda_{\pm,\mathrm{EP}} = \omega_0 \pm \mathrm{i}\sqrt{2\gamma\delta'} + \mathcal{O}(\delta')$. The eigenvalue sensitivity $\partial_{\delta'}\lambda$ is, hence, singular. In fact, the exceptional eigenvalue corresponds to a branch-point singularity in the parameter space with a self-intersecting Riemann sheet (**Figure 8**). Encircling an exceptional point through a suitable parameter variation consequently leads to chiral behavior, where the final state depends on the orientation of the encirclement (Doppler et al. 2016).

axially separated orifices acting as acoustic sources and sinks (**Figure 7**). This is a realization of the prototypical PT-symmetric system illustrated in **Figure 6** and represented, in simpler form, by Equation SB1. Loss is achieved through the insertion of resistive elements into the sink orifice that provide viscous dissipation; the gain orifice amplifies incident acoustic perturbations over a finite frequency range through interaction of the acoustic field with the sensitive shear layer, which forms at the upstream edge of the orifice. The PT symmetry of the two-orifice arrangement in the flow duct is verified based on the scattering matrix for the acoustic wave amplitudes. An analysis of the eigenvalues of the scattering matrix shows the transition between the symmetric and the broken phase (Aurégan & Pagneux 2017).

Exceptional points are found at the phase transition in PT-symmetric systems, but they are general features of parameter-dependent non-Hermitian operators (Moiseyev 2011, Heiss 2012). As such, it is perhaps not surprising that they can be found in various fluid systems, which typically are non-self-adjoint. In an earlier work, Jones (1988) studied exceptional points in the Orr–Sommerfeld equation for plane Poiseuille flow (although he did not refer to them as such) and

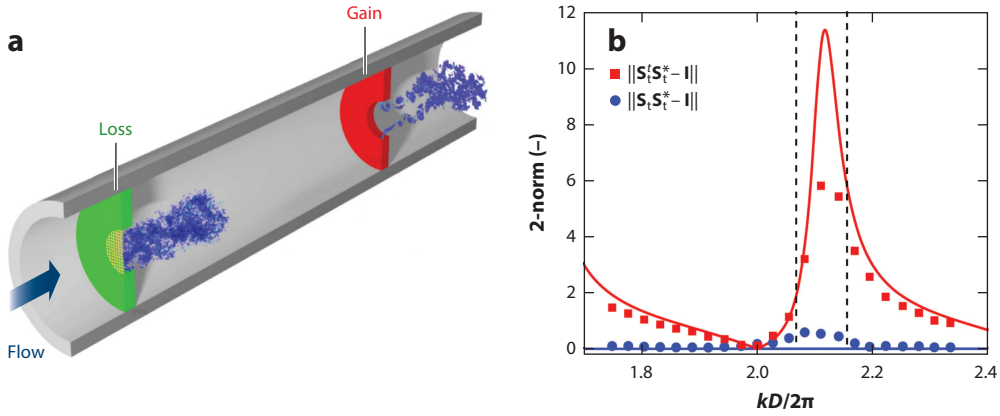

Figure 7

PT-symmetric aeroacoustic system with gain and loss elements in the form of orifices (Aurégan & Pagneux 2017). (*a*) Depiction of the experimental arrangement. Through interaction with the vortical hydrodynamic flow, the first and the second orifices dissipate and generate acoustic energy, respectively. (*b*) Norms associated with the scattering matrix, $\mathbf{S}_t$, of the system; the red symbols and line correspond to measured and modeled departure from acoustic energy conservation, respectively; blue symbols show departure from PT symmetry. Panels adapted with permission from Aurégan & Pagneux (2017); copyright 2017 American Physical Society. Abbreviation: PT, parity–time.

identified many of the key properties associated with them. Another example is magnetohydrodynamic flows that can be identified in connection with magnetorotational instabilities (Kirillov 2017). Mensah et al. (2018) identified exceptional points in a prototypical thermoacoustic system, found evidence for eigenvalue and mode coalescence, and argued that these are general features of this type of system. An intriguing aspect is that the modes that coalesce at an exceptional point in thermoacoustic systems can be assigned different physical mechanisms—one is of acoustic origin and the other is a mode intrinsic to the flame (Mensah et al. 2018); however, the formation of an exceptional point through the coalescence of two modes of acoustic origin was also observed (Orchini et al. 2020b). The presence of exceptional points, as shown by Mensah et al. (2018), physically explains the eigenvalue's extreme sensitivity found in thermoacoustic systems (Juniper & Sujith 2018, Sogaro et al. 2019, Ghani & Polifke 2021). In fact, the exceptional point affects the eigenvalue topology under parameter variation in a more global fashion, as **Figure 8** demonstrates. Operating a system coupled to an acoustic resonator at an exceptional point may provide the largest decay rate (Bourquard & Noiray 2019). Furthermore, as an exceptional point is a spectral singularity in parameter space, it limits the convergence of perturbation expansions (Orchini et al. 2020a). When a periodic parameter variation is considered, such as in the spectrum of pulsating Poiseuille flow, the presence of an exceptional point may lead to subharmonic eigenvalue orbits (Kern et al. 2022).

4. SERIES EXPANSION FOR SPECTRAL PROBLEMS

Research in both quantum and fluid mechanics has developed clever and hierarchical ways to reduce the complexity of a wide range of problems. Here, we review methods, borrowed from quantum physics, that were instrumental in solving problems in fluid dynamics. Moreover, since fluid mechanics problems are mathematically richer due to their dependence on a broader range of nonnormal operators, these adopted mathematical techniques have seen interesting and promising advancements, both in theory and applications.

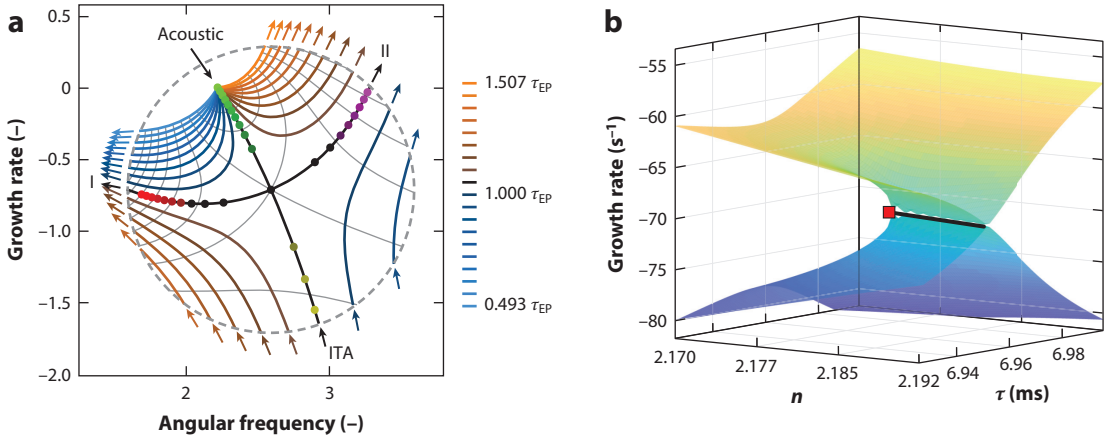

Figure 8

Exceptional points (EPs) in thermoacoustic systems: (*a*) Normalized eigenvalue trajectories around an EP when two system parameters are varied, here, feedback gain and time delay (τ) of the flame response model. The eigenvalue trajectories can be associated with two distinct origins when the flame feedback tends to zero, a purely acoustic mode and a flame-intrinsic mode (ITA). (*b*) Riemann surface for the growth rate as a function of the same two flame model parameters as in panel *a*. The exceptional point is marked with a red square. Panels adapted with permission from (*a*) Mensah et al. (2018), copyright 2018 Elsevier; and (*b*) Orchini et al. (2020b), copyright 2020 The Combustion Institute.

4.1. Degenerate Perturbation Theory

The objective of degenerate perturbation theory is to quantify changes in an eigenvalue due to an infinitesimally small perturbation to the underlying operator. Calculations of this type are based on perturbation methods. Perturbation theory for simple eigenvalues was pioneered for self-adjoint problems in acoustics by Lord Rayleigh (1896, section 90). A more general perturbation theory for degenerate eigenvalues was developed in quantum mechanics by Schrödinger (1928, pp. 64–76) to investigate the degeneracy of the hydrogen atom. This theory has to be further augmented since, in contrast to quantum mechanics, flow systems are not self-adjoint, and thus the adjoint eigenproblem has to be invoked to impose compatibility conditions. When the eigenvalue is twofold degenerate (but not defective), two solvability conditions need to be enforced, which yield a first-order correction to the eigenvalue, λ_1, of the form

$$\mathbf{X}\begin{bmatrix}\hat{\alpha}\\ \hat{\beta}\end{bmatrix} + \lambda_1 \mathbf{Y}\begin{bmatrix}\hat{\alpha}\\ \hat{\beta}\end{bmatrix} = 0, \qquad 9.$$

where $\mathbf{X}$ and $\mathbf{Y}$ are 2×2 matrices whose components are functions of the inner products between the unperturbed adjoint and direct eigenfunctions and of the operator perturbation (for the exact matrix expressions, see Magri 2019, section 3.3.1). Equation 9 constitutes an eigenvalue problem, with λ_1 as the eigenvalue and the coefficients of the unperturbed basis, $[\,\hat{\alpha}\;\;\hat{\beta}\,]^{\mathrm{T}}$, as the eigenvector.

If the perturbation breaks the symmetry of the system, the solution has two distinct eigenvalues, $\lambda_{1,1}$ and $\lambda_{1,2}$. The perturbation unfolds the degeneracy at first order, and the perturbed pair of eigenvalues, into which the degenerate unperturbed eigenvalue λ_0 splits, is given by $\lambda_0 + \varepsilon\lambda_{1,1}$ and $\lambda_0 + \varepsilon\lambda_{1,2}$, with ε as the perturbation parameter (**Figure 9**). Due to the splitting, one eigenvalue can become unstable (Mensah et al. 2019). The eigenvectors associated with $\lambda_{1,1}$ and $\lambda_{1,2}$, $[\,\hat{\alpha}_1\;\;\hat{\beta}_1\,]^{\mathrm{T}}$ and $[\,\hat{\alpha}_2\;\;\hat{\beta}_2\,]^{\mathrm{T}}$, respectively, indicate the directions along which the degenerate eigenspace unfolds. The elements of these eigenvectors are coordinates in the unperturbed degenerate eigenspace spanned by the unperturbed eigenfunctions. Equation 9 is a generalization

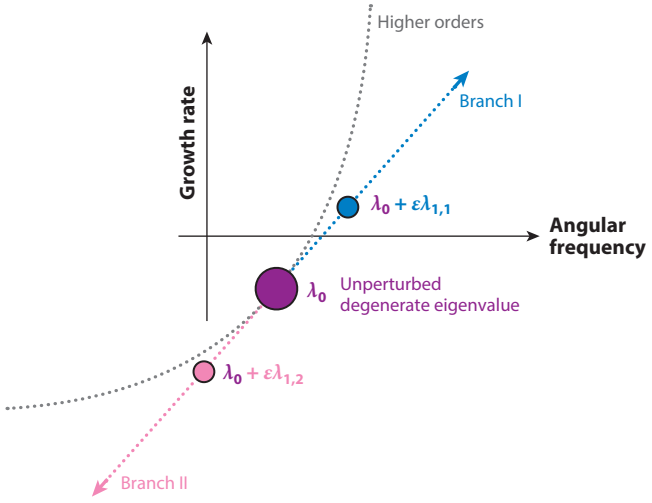

Figure 9

Eigenvalue splitting of a degenerate eigenvalue caused by an asymmetric perturbation. The eigenvalue in the unperturbed symmetric configuration (large circle) is twofold degenerate. An asymmetric perturbation unfolds the degenerate eigenvalue into two distinct eigenvalues (small circles) in two directions (branches I and II). The unfolding can have a destabilizing effect because the growth rate of a perturbed eigenvalue may increase.

of the eigenvalue sensitivity for nondegenerate problems (e.g., Luchini & Bottaro 2014) to the degenerate case, in which Equation 9 simplifies to the well-known first-order formula (eigenvalue drift) (for example, see Magri 2019, equation 101). Examples of degenerate problems are discussed in Section 3.1. A systematic framework for calculating higher-order expansions for non-Hermitian degenerate problems was recently proposed by Orchini et al. (2021).

4.2. The Semiclassical Limit: Wave Packet Pseudo-Modes

Many problems in fluid mechanics can be classified as spectral problems, where we seek solutions that are invariant under a time rate of change. These solutions often build the backbone of further analysis into flow processes and of a quantitative representation of the flow behavior (Schmid & Henningson 2001, Charru 2011). Stability problems constitute the majority of this category, but receptivity and sensitivity analyses can also be described as variations of spectral problems. In this section, the Jacobian of the eigenvalue problem of Equation 7 takes the form

$$\mathcal{L} = \sum_j \mathbf{Q}_j(\mathbf{x})\nabla_\epsilon^j, \qquad 10.$$

where $\nabla_\epsilon = i\epsilon\nabla$ denotes a scaled spatial gradient with ϵ as a small parameter. The small parameter can be physically motivated (such as the inverse Reynolds number) or geometrically induced (such as an aspect ratio or the inverse of a spatial extent). The variable coefficients $\mathbf{Q}_j(\mathbf{x})$ account for the spatial variations of mean flow quantities.

In the limit $\epsilon \to 0$, we can seek approximate invariant solutions of the form $\hat{\boldsymbol{\psi}} \sim \exp[\mathrm{i}S(\mathbf{x}/\epsilon)]$, with $S(\mathbf{x})$ the phase function. This approach is akin to a WKBJ (Wentzel—Kramers—Brillouin–Jeffreys) expansion (Bender & Orszag 1999), with $S(\mathbf{x})$ typically given by the geometric-optics

approximation or eikonal solution, following the standard expansion $S(\mathbf{x}) = S_0 + \nabla S_0^{\mathrm{T}}(\mathbf{x} - \mathbf{x}_0) + (\mathbf{x} - \mathbf{x}_0)^{\mathrm{T}} \nabla^2 S_0 (\mathbf{x} - \mathbf{x}_0) + \ldots$, where we have used the abbreviation $S_0 = S(\mathbf{x}_0)$ and done so equivalently for higher derivatives. By truncating the phase function at second order, we recognize that $\hat{\boldsymbol{\psi}}(\mathbf{x})$ assumes the shape of a wave packet centered about $\mathbf{x}_0$ with carrier wavenumber $\mathbf{k} = \nabla S$. With invariant solutions of this form, we have

$$\sum_j \mathbf{Q}_j(\mathbf{x}_0)\,(-\mathbf{k})^j = f(\mathbf{x}_0, \mathbf{k}) = \lambda, \qquad 11.$$

with the spectrum λ parameterized by both the primal variable $\mathbf{x}_0$ (the location of the wave packet) and the dual variable $\mathbf{k}$ (the scale of the wave packet). This represents an algebraic expression for the spectrum given by λ that depends on the position and scale of the eigenfunction only, linked via the details of the variable-coefficient operator $\mathcal{L}$. The function f is referred to as the symbol of the operator $\mathcal{L}$ (see, e.g., Dencker et al. 2004, Helffer 2008). For the invariant solution $\hat{\boldsymbol{\psi}}$ to take on the form of a wave packet, we have to require that $\nabla^2 S$ is negative definite. This condition is known as the twist condition (Trefethen 2005) and represents an admissibility condition for spatially compact invariants. For higher-dimensional problems, it is often more convenient to restate the twist condition in an equivalent form using Poisson brackets of the real and imaginary part of the symbol (Hörmander 1960). With the twist condition satisfied for a particular $\mathbf{x}_0$ and $\mathbf{k}$, the solution $\hat{\boldsymbol{\psi}}(\mathbf{x})$ is an exponentially good approximation of an invariant solution of $\mathcal{L}$ in the asymptotic limit of $\epsilon \to 0$ (Davies 1999, Dencker et al. 2004). This approximation is closely related to ϵ-pseudo-spectra (Trefethen & Embree 2005), an established tool to quantify stability behavior for nonnormal operators (Schmid 2007).

The mapping of the combined primal-dual space $(\mathbf{x}_0, \mathbf{k})$ under the symbol f onto the complex plane, while observing the twist condition, traces out the location of the spectrum in the limit $\epsilon \to 0$ and gives fast and approximate information about the spectral properties of the analyzed flow. A sketch of the procedural steps is given in **Figure 10**.

Not all mappings that satisfy the symbol and twist condition are admissible, as they also have to satisfy the boundary conditions. Adherence to this additional condition can be accomplished by enforcing the twist condition beyond mere negative definiteness: Instead, we impose a wave packet envelope that decays sufficiently rapidly to comply with boundary conditions. The minimal distance to the boundaries along the principal directions of $\nabla^2 S$ comes into play in this argument and introduces influences of the domain geometry on the spectral properties of the flow.

The above analysis can be made equivalent to a semiclassical analysis of quantum systems (Redparth 2001, Davies 1999, Helffer 2008), where the asymptotics of $\epsilon \to 0$ represent the limit process from a quantized to a classically continuous system. From a more mathematical point of view, the same process can be linked to pseudo-spectral theory in an asymptotic

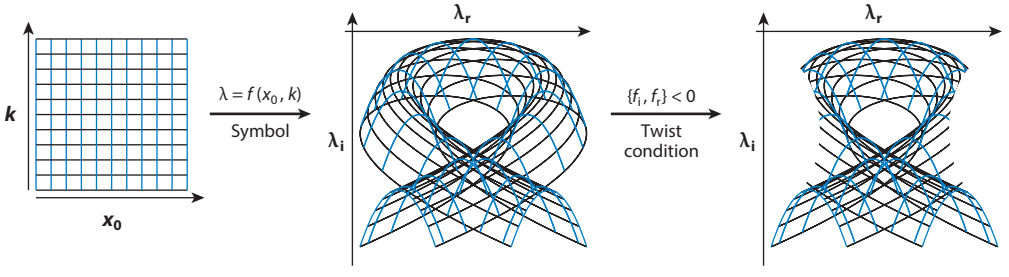

Figure 10

Sketch of spectral analysis using semiclassical techniques. The (primal-dual) physical wavenumber space is mapped under the symbol f onto the complex λ-plane. The twist condition is applied to the mapping to extract spatially compact wave packets.

($\epsilon \to 0$) sense, and to the microlocal analysis of differential and pseudo-differential operators (Dencker et al. 2004). Further connections can be made to the Wigner–Weyl transform, a mathematical technique to link operators to their phase space representations.

These semiclassically inspired techniques have been successfully applied to the spectral analysis of swept Hiemenz flow (Obrist & Schmid 2010) and the directivity problem in aero-acoustic scattering (Obrist 2009), as well as in the resolvent analysis of compressible flows (Dawson & McKeon 2019).

4.3. Wave Over-Reflection, Connection Formulae, and Tunneling

The tunneling effect is arguably one of the most surprising phenomena of early quantum mechanics, as it defies classical intuition. The wave-like solutions of the Schrödinger equation allow for scenarios where particles can be found on opposite sides of a potential well whose barrier height is (classically) too high, considering the energy level of the particle. A careful analysis using a composite ansatz of oscillatory and exponentially decaying local solutions demonstrates that a small but finite oscillatory solution exists outside the potential well, indicating a nonzero probability of finding a particle there.

This type of analysis, based on scattered and transmitted waves, has successfully been adopted in the analysis of acoustic resonance of subsonic jets (Towne et al. 2017), in the compressible flow through circular apertures (Fabre et al. 2020), and in general hydrodynamic stability (Chomaz et al. 1991, Pier & Huerre 2001, Chomaz 2005), most notably through the concept of wave over-reflection (Lindzen & Barker 1985, Lindzen 1988). Inviscid, incompressible shear flows are governed by a second-order Helmholtz equation, with an index of refraction whose sign depends on the details of the mean flow. In analogy to the Schrödinger equation, the Helmholtz equation supports propagating and evanescent wave solutions, and the role of the potential barriers is taken by regions close to the critical layers, where the phase speed of the wave equals the local mean flow velocity and where waves interact intensely with the mean flow. Mathematically, these regions act as turning points for the type of solutions (exponential or oscillatory) to the Helmholtz equation, and the question of hydrodynamic instability can be reduced to the solution of a scattering problem. Analogous to the quantum effect, vorticity wave flux from the inside of, say, a channel can tunnel through the critical regions and continue to propagate toward the wall (see **Figure 11** for a sketch). The matching across these two regions is given by specific connection formulae (Bender & Orszag 1999), equivalent to the tunneling solutions. Moreover, waves trapped between two critical layers, or between a critical layer and the wall, may amplify over the traveled distance and cause instabilities.

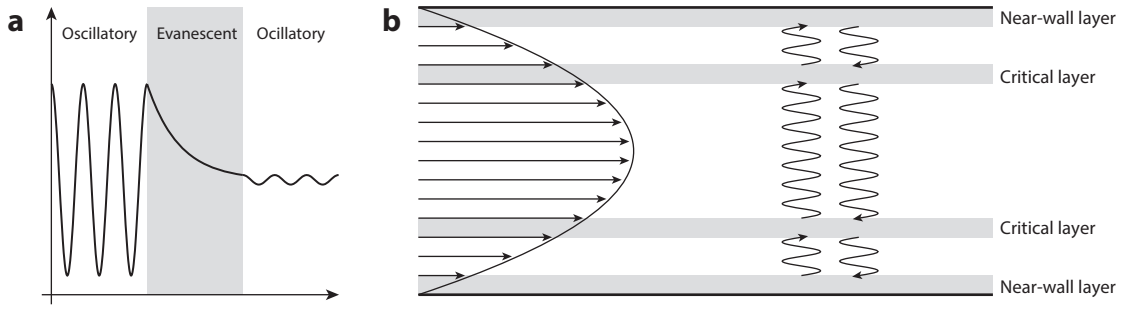

Figure 11

(*a*) Tunneling through an infinite potential well (*gray area*). (*b*) Hydrodynamic instability of plane Poiseuille flow as a wave scattering problem.

RAYLEIGH–TAYLOR INSTABILITY BY SEMICLASSICAL ANALYSIS

As a simple yet illustrative example of this type of spectral analysis, we consider the Rayleigh–Taylor instability (Helffer & Lafitte 2003) governed by the stability operator

$$\left[-\frac{1}{k^2}\frac{\mathrm{d}}{\mathrm{d}y}\bar{\rho}\frac{\mathrm{d}}{\mathrm{d}y}+\bar{\rho}+\bar{\rho}'\frac{g}{\lambda^2}\right]v=0 \qquad \rightarrow \qquad \left[-\epsilon^2\frac{\mathrm{d}}{\mathrm{d}y}\bar{\rho}\frac{\mathrm{d}}{\mathrm{d}y}+\bar{\rho}+\frac{1}{\delta}\bar{\rho}'\right]\exp(\mathrm{i}S/\epsilon)\hat{\boldsymbol{\psi}}\sim 0, \qquad \text{SB2.}$$

which we transformed using a WKBJ approach. In the above expression, the small parameter is $\epsilon = 1/k \equiv 1/\sqrt{k_x^2+k_z^2}$, the mean density is given by $\bar{\rho}(y)$, and δ is λ^2/g, with g the gravitational constant. From this second expression we can deduce the symbol $f(y_0, k_y)$ with $k_y = \mathrm{d}S/\mathrm{d}y$ for the Rayleigh–Taylor instability as

$$f(y_0,k_y)=-(1+k_y^2)^{-1}\frac{\bar{\rho}'(y_0)}{\bar{\rho}(y_0)}. \qquad \text{SB3.}$$

Varying (y_0, k_y) traces out the spectrum λ in the complex plane (see **Figure 10** for a conceptual sketch). Requiring compactness of the eigenfunctions via the twist condition produces a constraint on the quantity $(\bar{\rho}')^2 - \bar{\rho}\bar{\rho}''$, and together with an analysis of the type of extrema, we recover the conditions $\bar{\rho}' < 0$ and $\bar{\rho}\bar{\rho}''' - \bar{\rho}'\bar{\rho}'' > 0$, which are consistent with results obtained from a more traditional analysis.

The basic setup of this scenario and the existence of a wave-propagation region on the other side of an exponential region have been directly linked to the Rayleigh and Fjørtoft criterion for inviscid flow (Lindzen et al. 1980), and the requirement of a wave-sink beyond a critical layer has extended this concept to viscous flows where the near-wall boundary layer takes over this function. While for the inviscid case, the wave-sink is adjacent to the critical layer, in the viscous case the spatial separation of the wave-sink (near-wall layer) from the critical layer enters as a governing parameter for over-reflection and, thus, instability (**Figure 11**) (see the sidebar titled Rayleigh–Taylor Instability by Semiclassical Analysis). Based on this connection, instabilities in wall-bounded shear flows only exist for a rather narrow range of phase speeds (Lindzen & Barker 1985). A similar wave perspective has been applied to generic stability problems by Lifschitz & Hameiri (1991), who proposed a local WKBJ approach based on stagnation and equilibrium points to establish instability criteria.

The viewpoint of a hydrodynamic instability as an amplifying scattering problem has been applied to geophysical settings with stably stratified flows (for a review see, e.g., Lindzen 1988), leading to a more mechanistic explanation for the amplification of wave solutions. More recently, these results have been extended to incorporate transiently growing perturbations (Bakas & Farrell 2010). The role of critical layers and near-wall layers in hydrodynamic stability theory has been widely recognized and has fueled the development of sophisticated asymptotic tools, such as triple-deck theory (Stewartson 1974). Nonetheless, the quantum mechanical viewpoint via an analogy to tunneling furnishes an interpretable and alternative approach to understanding the rise of instabilities via wave amplification in a domain marked by multiple regions that act as partial reflectors, transmitters, or dampers.

5. SYNCHRONIZATION IN ACTIVE FLUIDS AND SPIN–ORBIT COUPLING

Active fluids exhibit uncommon behavior due to the presence of self-propelled and reactive particles. Their hydrodynamics is complicated by the fact that swarming and synchronization effects interact with more traditional behavior of the interstitial fluid. Colloids, granules, cells,

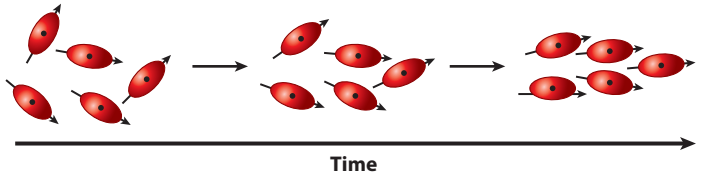

Figure 12

Interaction of active particles in an interstitial fluid, exhibiting flocking and orientation synchronization, which can be described by quantum mechanical spin–orbit coupling.

amoebas, and minute biomasses are but a few applications of active fluids, and an increased interest in this type of flows has spawned much research and analysis of flows with active biological matter (Saintillan 2018). Particle or agent models dominate the quantitative description of active fluids. Particle–particle as well as particle–fluid interactions are often modeled at a microscopic level and then amalgamated to the macroscopic level. This fine-to-coarse homogenization process invokes statistical arguments and introduces a variety of concepts from the field of many-particle quantum systems. This analogy from quantum systems, particularly spin–orbit coupling of many-electron systems, is of help in this step and provides a framework and formalism that can be transferred to the study of active flows (see the sidebar titled Active Swimmers' Equation with Pauli Matrices). The presence of active particles in an interstitial fluid introduces orientation as a new state variable and requires the modeling of particle interactions and their communication with the background fluid. Experiments have reported the formation of particle clusters and aggregate coherent states brought about by shear alignment and particle-to-particle synchronization (see **Figure 12** for a sketch of this phenomenon).

A similar approach can be taken for any fluid system where active agents (from biomatter at the cellular level to polymers, and from colloids to dry granular assemblies) play an important

ACTIVE SWIMMERS' EQUATION WITH PAULI MATRICES

A quantitative description of this motion starts with a single-particle Hamiltonian

$$\mathcal{H} = \frac{1}{2}\left[\boldsymbol{\sigma}\cdot\nabla + m(I-\sigma_z) - \frac{1}{\kappa}\nabla^2\right] \qquad \text{with} \qquad \boldsymbol{\sigma}\cdot\nabla = \sigma_x\partial_x + \sigma_y\partial_y, \qquad \text{SB4.}$$

where $\boldsymbol{\sigma}$ denotes the vector of Pauli matrices (σ_x, σ_y) and $1/\kappa$ represents a diffusion constant. Spin–orbit coupling is described by $\boldsymbol{\sigma}\cdot\nabla$, rotational noise is modeled by $m(I-\sigma_z)$, and translational noise (along the particle's path) is captured by the diffusive term ∇^2/κ. In the above expression, we restrict ourselves to 2D motion in the x–y-plane, with particle rotations about the z-axis; furthermore, we take $\hbar = 1$. A formulation as a Schrödinger system, using a rotation of the time-axis from the real t to the complex it, allows one to derive an advective-diffusive equation for the active-fluid model. The close link between the Schrödinger formalism for quantum systems and a statistical description of fluid processes can be exploited to arrive at a well-founded model for incorporating active particles into a general hydrodynamic formulation. From the above Hamiltonian, by modeling spin–orbit coupling via two relaxation terms, namely, momentum dissipation and rotational alignment, one can derive a governing equation via a Fokker–Planck formulation. This governing equation takes on the form of a stochastic Langevin equation (Loewe et al. 2018). In a final step, a scaling from a single-particle Hamiltonian to an N-particle system, together with the associated statistical notion, yields a system of governing equations that accurately describes fluids in which embedded active agents affect the flow behavior significantly and nontrivially.

role and where flocking and synchronization effects give rise to coherent motion and aggregation. In these cases, quantum mechanical descriptions, paired with a statistical homogenization step, prove advantageous in the derivation of governing equations and the modeling of complex flow behavior.

6. CONCLUSIONS

Quantum mechanics, with its focus on the spectral analysis of operators linked to physical variables, has much to offer to fluid dynamicists with an interest in the quantitative description of linear flow behavior for a wide range of applications. While there can be marked differences between quantum mechanical and fluid dynamical configurations, a transfer of methodology or a modification of techniques can often lead to a more elegant or compact solution, to more insight into the underlying flow physics, or to an alternative and fresh perspective on a well-studied problem. In this review, we have touched on a few fundamental concepts that are routinely applied in quantum systems but are less commonly brought to bear on fluid problems, and we have demonstrated their potential when investigating linear flow behavior. Concentrating on spectral analysis, various series expansions, symmetry and symmetry-breaking, eigenvalue degeneracies, sensitivities, and exceptional points, as well as on spectral approximations, scattering problems and synchronizing many-body systems, we have illustrated the richness of quantum mechanical approaches that can be harnessed to aid and guide the mathematical analysis of fluid systems. We hope that, by pointing out commonalities between these two related subjects and their mathematical procedures, we entice young and seasoned researchers alike into adopting some of these techniques and skills into their classical arsenal of tools.

SUMMARY POINTS

1. Spectral problems are at the heart of both quantum mechanics and fluid stability problems even though most fluid systems are governed by nonnormal operators (in contrast to most quantum systems). The spectra of fluid systems can be expanded and approximated by utilizing, and extending, many techniques from quantum mechanics.
2. Two-state systems, often encountered in fluid dynamics, can be concisely formulated by introducing a qubit representation on a Bloch sphere. This can resolve ambiguities in the state-space representation. We presented an example of an industrial gas turbine where a Bloch sphere representation provided physical insights into the intrinsic acoustic instability.
3. Solution strategies based on path integrals and Dyson expansions, together with their approximations, can be applied to a class of acoustic problems to efficiently and accurately compute the dominant physical solutions, order by order.
4. Symmetry and symmetry-breaking are key features in either field. They can be linked to the coalescence of eigenvalues, the rise of eigenvalue degeneracies, and to exceptional points. These points influence the topology of the spectrum, and explain the extreme eigenvalue sensitivity for a class of linear systems. This also has significant implications for flow control.
5. Approximate spectral information about linear fluid systems can be gained by series expansions or asymptotic perturbation approaches (semiclassical analysis), avoiding or supplementing large-scale computations.

6. Quantum analogies (such as interacting many-body systems using Hamiltonians) can be harnessed, together with a statistical homogenization process, to rigorously derive rheological models for particle-laden and active fluids.

FUTURE ISSUES

1. Quantitative analysis, and in particular spectral analysis, of increasingly complex flows will need to embrace more nontraditional techniques in the form of approximate tools, novel state-representations, or variational approaches.
2. Mathematical techniques from quantum mechanics may also be incorporated into large-scale scientific computing algorithms to improve efficiency and guide convergence, for example, in the form of Bloch waves for symmetric configurations.
3. Approximate and perturbation analysis can be utilized in rapid prototyping during the design of flow devices. The optimization of the performance of fluid systems can also benefit from the type of analysis presented in this review.
4. Exceptional points giving rise to intriguing, unexpected features have been found in a variety of areas governed by wave-like dynamics (e.g., optics, photonics, acoustics). Systematically locating and characterizing these spectral singularities in flow dynamical systems may reveal novel phenomena and provide opportunities for new applications.

DISCLOSURE STATEMENT

The authors are not aware of any biases that might be perceived as affecting the objectivity of this review.

ACKNOWLEDGMENTS

We are grateful to Oleg Kirillov, Flavio Giannetti, Nicolas Noiray, Giulio Ghirardo, Andrea Giusti, and Tim Colonius for their comments on a draft of this manuscript. We thank A. Jain for assisting with **Figure 2*d***. L.M. gratefully acknowledges financial support from the European Research Council Starting Grant PhyCo 94938 and the Royal Academy of Engineering Research Fellowships scheme (2016–2021).

LITERATURE CITED

Ahn B, Indlekofer T, Dawson J, Worth N. 2021. Transient thermo-acoustic responses of methane/hydrogen flames in a pressurized annular combustor. *J. Eng. Gas Turbines Power* 144:011018

Arecchi FT, Courtens E, Gilmore R, Thomas H. 1972. Atomic coherent states in quantum optics. *Phys. Rev. A* 6(6):2211–37

Aurégan Y, Pagneux V. 2017. PT-symmetric scattering in flow duct acoustics. *Phys. Rev. Lett.* 118(17):174301

Bakas NA, Farrell BF. 2010. The role of nonnormality in overreflection theory. *J. Atmos. Sci.* 67:2547–58

Barenblatt GI. 1996. *Scaling, Self-Similarity, and Intermediate Asymptotics*. Cambridge, UK: Cambridge Univ. Press

Bauerheim M, Cazalens M, Poinsot T. 2015. A theoretical study of mean azimuthal flow and asymmetry effects on thermo-acoustic modes in annular combustors. *Proc. Combust. Inst.* 35:3219–27

Bauerheim M, Nicoud F, Poinsot T. 2016. Progress in analytical methods to predict and control azimuthal combustion instability modes in annular chambers. *Phys. Fluids* 28(2):021303

Bender CM. 2019. *PT Symmetry: In Quantum and Classical Physics*. London: World Sci.

Bender CM, Boettcher S. 1998. Real spectra in non-Hermitian Hamiltonians having PT symmetry. *Phys. Rev. Lett.* 80(24):5243–46

Bender CM, Orszag SA. 1999. *Advanced Mathematical Methods for Scientists and Engineers I: Asymptotic Methods and Perturbation Theory*. New York: Springer

Berry MV, Wilkinson M. 1984. Diabolical points in the spectra of triangles. *Proc. R. Soc. A* 392(1802):15–43

Birkhoff G, Von Neumann J. 1936. The logic of quantum mechanics. *Ann. Math.* 37(4):823–43

Bloch F. 1929. Über die Quantenmechanik der Elektronen in Kristallgittern. *Z. Phys.* 52(7–8):555–600

Bloch F. 1946. Nuclear induction. *Phys. Rev.* 70(7–8):460

Bluman G, Kumei S. 1996. *Symmetries and Differential Equations*. New York: Springer

Bothien M, Noiray N, Schuermans B. 2015. Analysis of azimuthal thermo-acoustic modes in annular gas turbine combustion chambers. *J. Eng. Gas Turbines Power* 137:061505

Bourgouin JF, Durox D, Moeck JP, Schuller T, Candel S. 2013. Self-sustained instabilities in an annular combustor coupled by azimuthal and longitudinal acoustic modes. In *Proceedings of the ASME Turbo Expo 2013: Turbine Technical Conference and Exposition*, Vol. 1B: *Combustion, Fuels and Emissions*, Pap. V01BT04A007. New York: ASME

Bourgouin JF, Durox D, Moeck JP, Schuller T, Candel S. 2015. A new pattern of instability observed in an annular combustor: the slanted mode. *Proc. Combust. Inst.* 35(3):3237–44

Bourquard C, Noiray N. 2019. Stabilization of acoustic modes using Helmholtz and Quarter-Wave resonators tuned at exceptional points. *J. Sound Vib.* 445:288–307

Bridges J, Wernet M. 2002. *Turbulence measurements of separate flow nozzles with mixing enhancement features*. Paper presented at 8th AIAA/CEAS Aeroacoustics Conference & Exhibit, Breckenridge, CO, AIAA Pap. 2002-2484

Bush JW. 2015. Pilot-wave hydrodynamics. *Annu. Rev. Fluid Mech.* 47:269–92

Candel S. 2002. Combustion dynamics and control: progress and challenges. *Proc. Combust. Inst.* 29:1–28

Cantwell BJ. 2002. *Introduction to Symmetry Analysis*. Cambridge, UK: Cambridge Univ. Press

Charru F. 2011. *Hydrodynamic Instabilities*. Cambridge, UK: Cambridge Univ. Press

Chomaz JM. 2005. Global instabilities in spatially developing flows: non-normality and nonlinearity. *Annu. Rev. Fluid Mech.* 37:357–92

Chomaz JM, Huerre P, Redekopp L. 1991. A frequency selection criterion in spatially developing flows. *Stud. Appl. Math.* 84:119–44

Couder Y, Fort E, Gautier CH, Boudaoud A. 2005. From bouncing to floating: noncoalescence of drops on a fluid bath. *Phys. Rev. Lett.* 94(17):177801

Crawford JD, Knobloch E. 1991. Symmetry and symmetry-breaking bifurcations in fluid dynamics. *Annu. Rev. Fluid Mech.* 23:341–87

Culick FEC. 2006. *Unsteady motions in combustion chambers for propulsion systems*. Tech. Rep. AG-AVT-039, RTO (Res. Technol. Organ.), NATO (N. Atl. Treaty Organ.), Neuilly-sur-Seine, France

Davey A. 1978. On the stability of flow in an elliptic pipe which is nearly circular. *J. Fluid Mech.* 87(2):233–41

Davey A, Salwen H. 1994. On the stability of flow in an elliptic pipe which is nearly circular. *J. Fluid Mech.* 281:357–69

Davies E. 1999. Semi-classical states for non-self-adjoint Schrödinger operators. *Commun. Math. Phys.* 200:35–41

Dawson S, McKeon BJ. 2019. On the shape of resolvent modes in wall-bounded turbulence. *J. Fluid Mech.* 877:682–716

Dencker N, Sjöstrand J, Zworski M. 2004. Pseudo-spectra of semi-classical (pseudo) differential operators. *Commun. Pure Appl. Math.* 57:384–415

Dirac PAM. 1930. *The Principles of Quantum Mechanics*. Oxford: Oxford Univ. Press

Doppler J, Mailybaev AA, Böhm J, Kuhl U, Girschik A, et al. 2016. Dynamically encircling an exceptional point for asymmetric mode switching. *Nature* 537(7618):76–79

Dowling AP, Mahmoudi Y. 2015. Combustion noise. *Proc. Combust. Inst.* 35:65–100

Durán I, Moreau S, Poinsot T. 2013. Analytical and numerical study of combustion noise through a subsonic nozzle. *AIAA J.* 51:42–52
Duran I, Morgans AS. 2015. On the reflection and transmission of circumferential waves through nozzles. *J. Fluid Mech.* 773:137–53
Fabre D, Longobardi R, Citro V, Luchini P. 2020. Acoustic impedance and hydrodynamic instability of the flow through a circular aperture in a thick plate. *J. Fluid Mech.* 885:A11
Faure-Beaulieu A, Indlekofer T, Dawson JR, Noiray N. 2021. Imperfect symmetry of real annular combustors: beating thermoacoustic modes and heteroclinic orbits. *J. Fluid Mech.* 925:R1
Fedorov A. 2011. Transition and stability of high-speed boundary layers. *Annu. Rev. Fluid Mech.* 43:79–95
Floquet G. 1883. Sur les équations différentielles linéaires à coefficients périodiques. *Ann. Sci. l'Éc. Norm. Supér. Sér. 2* 12:47–88
Ghani A, Polifke W. 2021. An exceptional point switches stability of a thermoacoustic experiment. *J. Fluid Mech.* 920:R3
Ghirardo G, Bothien MR. 2018. Quaternion structure of azimuthal instabilities. *Phys. Rev. Fluids* 3(11):113202
Ghirardo G, Boudy F, Bothien MR. 2018. Amplitude statistics prediction in thermoacoustics. *J. Fluid Mech.* 844:216–46
Ghirardo G, Di Giovine C, Moeck JP, Bothien MR. 2019. Thermoacoustics of can-annular combustors. *J. Eng. Gas Turbines Power* 141:011007
Ghirardo G, Gant F. 2019. Background noise pushes azimuthal instabilities away from spinning states. arXiv:1904.00213 [physics.flu-dyn]. **https://doi.org/10.48550/arXiv.1904.00213**
Ghirardo G, Gant F. 2021. Averaging of thermoacoustic azimuthal instabilities. *J. Sound Vib.* 490:115732
Ghirardo G, Juniper MP. 2013. Azimuthal instabilities in annular combustors: standing and spinning modes. *Proc. R. Soc. A* 469:20130232
Ghirardo G, Juniper MP, Moeck JP. 2016. Weakly nonlinear analysis of thermoacoustic instabilities in annular combustors. *J. Fluid Mech.* 805:52–87
Giusti A, Worth NA, Mastorakos E, Dowling AP. 2017. Experimental and numerical investigation into the propagation of entropy waves. *AIAA J.* 55(2):446–58
Golubitsky M, Stewart I. 1985. Hopf bifurcation in the presence of symmetry. *Arch. Ratio. Mech. Anal.* 87:107–65
Griffiths DJ. 1995. *Introduction to Quantum Mechanics*. Upper Saddle River, NJ: Prentice-Hall
Güttel S, Tisseur F. 2017. The nonlinear eigenvalue problem. *Acta Numer.* 26:1–94
Hamermesh M. 1989. *Group Theory and Its Application to Physical Problems*. New York: Dover
Heiss WD. 2004. Exceptional points of non-Hermitian operators. *J. Phys. A* 37(6):2455–64
Heiss WD. 2012. The physics of exceptional points. *J. Phys. A* 45:444016
Helffer B. 2008. Four lectures in semiclassical analysis for non-self-adjoint problems with applications to hydrodynamic instability. In *Pseudo-Differential Operators Quantization and Signals*, ed. HG Feichtinger, B Helffer, MP Lamoureux, N Lerner, J Toft, pp. 35–77. Berlin: Springer-Verlag
Helffer B, Lafitte O. 2003. Asymptotic growth rate for the linearized Rayleigh equation for the Rayleigh–Taylor instability. *Asymptot. Anal.* 33:189–235
Herbert T. 1988. Secondary instability of boundary layers. *Annu. Rev. Fluid Mech.* 20:487–526
Hörmander L. 1960. Differential equations without solutions. *Math. Ann.* 140:169–73
Howe MS, Liu JTC. 1977. The generation of sound by vorticity waves in swirling duct flows. *J. Fluid Mech.* 81:369–83
Huerre P, Monkewitz PA. 1990. Local and global instabilities in spatially developing flows. *Annu. Rev. Fluid Mech.* 22:473–537
Ihme M. 2017. Combustion and engine-core noise. *Annu. Rev. Fluid Mech.* 49:277–310
Inui T, Tanabe Y, Onodera Y. 1990. *Group Theory and Its Applications in Physics*. Berlin: Springer-Verlag
Jain A, Magri L. 2022. A physical model for indirect noise in non-isentropic nozzles: transfer functions and stability. *J. Fluid Mech.* 935:A33
Joannopoulos JD, Johnson SG, Winn JN, Meade RD. 2008. *Photonic Crystals*. Princeton, NJ: Princeton Univ. Press. 2nd ed.
Jones CA. 1988. Multiple eigenvalues and mode classification in plane Poiseuille flow. *Q. J. Mech. Appl. Math.* 41(3):363–82

Jovanović MR. 2021. From bypass transition to flow control and data-driven turbulence modeling: an input–output viewpoint. *Annu. Rev. Fluid Mech.* 53:311–45

Juniper MP, Sujith RI. 2018. Sensitivity and nonlinearity of thermocoustic oscillations. *Annu. Rev. Fluid Mech.* 50:661–89

Kato T. 1980. *Perturbation Theory for Linear Operators*. New York: Springer. 2nd ed.

Kern JS, Hanifi A, Henningson DS. 2022. Subharmonic eigenvalue orbits in the spectrum of pulsating Poiseuille flow. *J. Fluid Mech.* 945:A11

Kerswell RR. 2018. Nonlinear nonmodal stability theory. *Annu. Rev. Fluid Mech.* 50:319–45

Kirillov ON. 2017. Singular diffusionless limits of double-diffusive instabilities in magnetohydrodynamics. *Proc. R. Soc. A* 473(2205):20170344

Kirillov ON. 2021. *Nonconservative Stability Problems of Modern Physics*. Berlin: De Gruyter. 2nd ed.

Kopiev VF, Ostrikov NN, Chernyshev SA, Elliott JW. 2004. Aeroacoustics of supersonic jet issued from corrugated nozzle: new approach and prospects. *Int. J. Aeroacoust.* 3(3):199–228

Kristiansen UR, Wiik GA. 2007. Experiments on sound generation in corrugated pipes with flow. *J. Acoust. Soc. Am.* 121(3):1337–44

Kronig RD, Penney WG. 1931. Quantum mechanics of electrons in crystal lattices. *Proc. R. Soc. A* 130:499–513

Laera D, Schuller T, Prieur K, Durox D, Camporeale SM, Candel S. 2017. Flame describing function analysis of spinning and standing modes in an annular combustor and comparison with experiments. *Combust. Flame* 184:136–52

Lajús FC, Sinha A, Cavalieri AVG, Deschamps CJ, Colonius T. 2019. Spatial stability analysis of subsonic corrugated jets. *J. Fluid Mech.* 876:766–91

Lieuwen TC, Yang V. 2005. *Combustion Instabilities in Gas Turbine Engines: Operational Experience, Fundamental Mechanisms, and Modeling*. Reston, VA: AIAA

Lifschitz A, Hameiri E. 1991. Local stability conditions in fluid dynamics. *Phys. Fluids* 3:2644

Lindzen RS. 1988. Instability of plane parallel shear flow (toward a mechanistic picture of how it works). *Pure Appl. Geophys.* 126:103–21

Lindzen RS, Barker JW. 1985. Instability and wave over-reflection in stably stratified shear flow. *J. Fluid Mech.* 151:189–217

Lindzen RS, Farrell BF, Tung KK. 1980. The concept of wave overreflection and its application to baroclinic instability. *J. Atmos. Sci.* 37:44–63

Loewe B, Souslov A, Goldbart PM. 2018. Flocking from a quantum analogy: spin-orbit coupling in an active fluid. *New J. Phys.* 20:013020

Luchini P, Bottaro A. 2014. Adjoint equations in stability analysis. *Annu. Rev. Fluid Mech.* 46:493–517

Lyu B, Dowling AP. 2019. Temporal stability analysis of jets of lobed geometry. *J. Fluid Mech.* 860:5–39

Magri L. 2017. On indirect noise in multi-component nozzle flows. *J. Fluid Mech.* 828:R2

Magri L. 2019. Adjoint methods as design tools in thermoacoustics. *Appl. Mech. Rev.* 71(2):020801

Magri L, Bauerheim M, Nicoud F, Juniper MP. 2016. Stability analysis of thermo-acoustic nonlinear eigenproblems in annular combustors. Part I. Sensitivity. *J. Comput. Phys.* 325:411–21

Marble FE, Candel SM. 1977. Acoustic disturbance from gas non-uniformities convected through a nozzle. *J. Sound Vibr.* 55(2):225–43

Mazur M, Kwah YH, Indlekofer T, Dawson JR, Worth NA. 2021. Self-excited longitudinal and azimuthal modes in a pressurised annular combustor. *Proc. Combust. Inst.* 38(4):5997–6004

Mensah GA, Campa G, Moeck JP. 2016. Efficient computation of thermoacoustic modes in industrial annular combustion chambers based on Bloch-wave theory. *J. Eng. Gas Turbines Power* 138(8):081502

Mensah GA, Magri L, Orchini A, Moeck JP. 2019. Effects of asymmetry on thermoacoustic modes in annular combustors: a higher-order perturbation study. *J. Eng. Gas Turbines Power* 141(4):041030

Mensah GA, Magri L, Silva C, Buschmann P, Moeck J. 2018. Exceptional points in the thermoacoustic spectrum. *J. Sound Vibr.* 433:124–28

Miri MA, Alú A. 2019. Exceptional points in optics and photonics. *Science* 363(6422):eaar7709

Moarref R, Jovanović MR. 2010. Controlling the onset of turbulence by streamwise travelling waves. Part 1. Receptivity analysis. *J. Fluid Mech.* 663:70–99

Moeck JP, Paul M, Paschereit CO. 2010. Thermoacoustic instabilities in an annular Rijke tube. In *ASME Turbo Expo 2010: Power for Land, Sea, and Air*, Vol. 2: *Combustion, Fuels and Emissions*, pp. 1219–32. New York: ASME

Moiseyev N. 2011. *Non-Hermitian Quantum Mechanics*. Cambridge, UK: Cambridge Univ. Press

Morgans AS, Duran I. 2016. Entropy noise: a review of theory, progress and challenges. *Int. J. Spray Combust. Dyn.* 8(4):285–98

Murthy SR, Sayadi T, LeChenadec V, Schmid PJ, Bodony D. 2019. Analysis of degenerate mechanisms triggering finite-amplitude thermo-acoustic oscillations in annular combustors. *J. Fluid Mech.* 881:384–419

Nicoud F, Benoit L, Sensiau C, Poinsot T. 2007. Acoustic modes in combustors with complex impedances and multidimensional active flames. *AIAA J.* 45(2):426–41

Noether E. 1918. Invariante Variationsprobleme. *Nachr. Ges. Wiss. Gött. Math.-Phys. Klasse* 1918:235–57

Noiray N, Bothien M, Schuermans B. 2011. Investigation of azimuthal staging concepts in annular gas turbines. *Combust. Theory Model.* 15(5):585–606

Noiray N, Schuermans B. 2013. On the dynamic nature of azimuthal thermoacoustic modes in annular gas turbine combustion chambers. *Proc. R. Soc. A* 469(2151):20120535

Obrist D. 2009. Directivity of acoustic emissions from wave packets to the far field. *J. Fluid Mech.* 640:165–86

Obrist D, Schmid PJ. 2010. Algebraically decaying modes and wavepacket pseudomodes in swept Hiemenz flow. *J. Fluid Mech.* 643:309–32

Orchini A, Magri L, Silva CF, Mensah GA, Moeck JP. 2020a. Degenerate perturbation theory in thermoacoustics: high-order sensitivities and exceptional points. *J. Fluid Mech.* 903:A37

Orchini A, Mensah GA, Moeck JP. 2021. Perturbation theory of nonlinear, non-self-adjoint eigenvalue problems: semisimple eigenvalues. *J. Sound Vibr.* 507:116150

Orchini A, Silva CF, Mensah GA, Moeck JP. 2020b. Thermoacoustic modes of intrinsic and acoustic origin and their interplay with exceptional points. *Combust. Flame* 214:251–62

Pier B, Huerre P. 2001. Nonlinear self-sustained structures and fronts in spatially developing wake flows. *J. Fluid Mech.* 435:145–74

Poignand G, Olivier C, Penelet G. 2021. Parity-time symmetric system based on the thermoacoustic effect. *J. Acoust. Soc. Am.* 149(3):1913–22

Ran W, Zare A, Jovanović MR. 2021. Model-based design of riblets for turbulent drag reduction. *J. Fluid Mech.* 906:A7

Rayleigh L. 1878. The explanation of certain acoustical phenomena. *Nature* 18:319–21

Rayleigh L. 1896. *The Theory of Sound*, Vol. 2. London: Macmillan. 2nd ed.

Redparth P. 2001. Spectral properties of non-self-adjoint operators in the semi-classical regime. *J. Differ. Equ.* 177:307–30

Rigas G, Esclapez L, Magri L. 2017. Symmetry breaking in a 3D bluff-body wake. arXiv:1703.07405 [physics.flu-dyn] **https://doi.org/10.48550/arXiv.1703.07405**

Rigas G, Morgans AS, Brackston RD, Morrison JF. 2015. Diffusive dynamics and stochastic models of turbulent axisymmetric wakes. *J. Fluid Mech.* 778:R2

Rigas G, Pickering EM, Schmidt OT, Nogueira PA, Cavalieri AV, et al. 2019. *Streaks and coherent structures in jets from round and serrated nozzles*. Paper presented at 25th AIAA/CEAS Aeroacoustics Conference, Delft, The Netherlands, AIAA Pap. 2019-2597

Russo S, Fabre D, Giannetti F, Luchini P. 2016. The speed of sound in periodic ducts. *J. Sound Vib.* 361:243–50

Saintillan D. 2018. Rheology of active fluids. *Annu. Rev. Fluid Mech.* 50:563–92

Sakurai JJ, Napolitano J. 2011. *Modern Quantum Mechanics*. Boston: Addison-Wesley. 2nd ed.

Schmid PJ. 2007. Nonmodal stability theory. *Ann. Rev. Fluid Mech.* 39:129–62

Schmid PJ, Fosas de Pando M, Peake N. 2017. Stability analysis for *n*-periodic arrays of fluid systems. *Phys. Rev. Fluids* 2(11):113902

Schmid PJ, Henningson DS. 2001. *Stability and Transition of Shear Flows*. New York: Springer

Schrödinger E. 1928. *Collected Papers on Wave Mechanics*. London: Blackie & Son

Schuermans B, Paschereit C, Monkewitz P. 2006. *Non-linear combustion instabilities in annular gas-turbine combustors*. Paper presented at 44th AIAA Aerospace Sciences Meeting and Exhibit, Reno, NV, AIAA Pap. 2006-549

Seyranian AP, Kirillov ON, Mailybaev AA. 2005. Coupling of eigenvalues of complex matrices at diabolic and exceptional points. *J. Phys. A* 38(8):1723

Seyranian AP, Mailybaev AA. 2003. *Multiparameter Stability Theory with Mechanical Applications*. London: World Sci.

Sinha A, Gudmundsson K, Xia H, Colonius T. 2016. Parabolized stability analysis of jets from serrated nozzles. *J. Fluid Mech.* 789:36–63

Sogaro FS, Schmid PJ, Morgans AS. 2019. Thermoacoustic interplay between intrinsic thermoacoustic and acoustic modes: non-normality and high sensitivities. *J. Fluid Mech.* 878:190–220

Steen LA. 1973. Highlights in the history of spectral theory. *Am. Math. Mon.* 80(4):359–81

Stewartson K. 1974. Multistructured boundary layers on flat plates and related bodies. *Adv. Appl. Mech.* 14:145–239

Stuart JT. 1971. Nonlinear stability theory. *Annu. Rev. Fluid Mech.* 3:347–70

Theofilis V. 2011. Global linear instability. *Annu. Rev. Fluid Mech.* 43:319–52

Towne A, Cavalieri AVG, Jordan P, Colonius T, Schmidt O, et al. 2017. Acoustic resonance in the potential core of subsonic jets. *J. Fluid Mech.* 825:1113–52

Trefethen LN. 2005. Wave packet pseudomodes of variable coefficient differential operators. *Proc. R. Soc. A* 461:3099–122

Trefethen LN, Embree M. 2005. *Spectra and Pseudospectra: The Behavior of Nonnormal Matrices and Operators*. Princeton, NJ: Princeton University Press

Trefethen LN, Trefethen AE, Reddy SC, Driscoll TA. 1993. Hydrodynamic stability without eigenvalues. *Science* 261:578–84

van Gils SA, Mallet-Paret J. 1986. Hopf bifurcation and symmetry: travelling and standing waves on the circle. *Proc. R. Soc. Edinburgh. A* 104(3–4):279–307

von Neumann J, Wigner EP. 1929. Über das Verhalten von Eigenwerten bei adiabatischen Prozessen. *Phys. Z.* 30:467–70

von Saldern JGR, Moeck JP, Orchini A. 2021. Nonlinear interaction between clustered unstable thermoacoustic modes in can-annular combustors. *Proc. Combust. Inst.* 38(4):6145–53

Wolf P, Staffelbach G, Gicquel LY, Müller JD, Poinsot T. 2012. Acoustic and large eddy simulation studies of azimuthal modes in annular combustion chambers. *Combust. Flame* 159(11):3398–413

Worth NA, Dawson JR. 2013. Modal dynamics of self-excited azimuthal instabilities in an annular combustion chamber. *Combust. Flame* 160(11):2476–89

Wu Y, Yang M, Sheng P. 2018. Perspective: Acoustic metamaterials in transition. *J. Appl. Phys.* 123(9):090901

Annual Review of Fluid Mechanics

Volume 55, 2023

Contents

Indexes

Errata

An online log of corrections to *Annual Review of Fluid Mechanics* articles may be found at http://www.annualreviews.org/errata/fluid